STUDY AND ANALYSIS OF MULTI-RING SILICA PHOTONIC CRYSTAL FIBERS FOR BROADBAND SPECTRA GENERATION

A Thesis report is submitted in partial fulfillment of the requirements for the award of Degree of Bachelor of Science in Electrical and Electronic Engineering.

Submitted by

MD SIZAN 213-33-1420

Asibur Rahman 213-33-1451

Supervised by

Dr. Mohammad Rezaul Karim

Professor

Department of Electrical and Electronic Engineering

Department of Electrical and Electronic Engineering

Faculty of Engineering

DAFFODIL INTERNATIONAL UNIVERSITY

OCTOBER, 2025

DECLARATION

I hereby declare that this thesis **Study and Analysis of Multi-Ring Silica Photonic Crystal Fibers for Broadband Spectra Generation** represents my own work which has been done in the laboratories of the Department of Electrical and Electronic Engineering under the Faculty of Engineering of Daffodil International University in partial fulfillment of the requirements for the degree of Bachelor of Science in Electrical and Electronic Engineering, and has not been previously included in a thesis or dissertation submitted to this or any other institution for a degree, diploma or other qualifications. I have attempted to identify all the risks related to this research that may arise in conducting this research, obtained the relevant ethical and/or safety approval (where applicable), and acknowledged my obligations and the rights of the participants.

Signature of the candidates

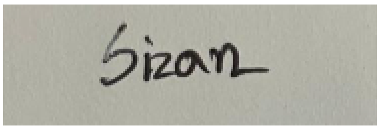

____

Name: MD SIZAN

ID: 213-33-1420

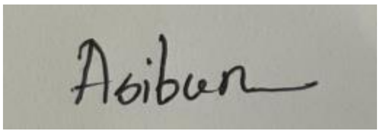

____

Name: Asibur Rahman

ID: 213-33-1451

APPROVAL

The thesis entitled **Study and Analysis of Multi-Ring Silica Photonic Crystal Fibers for Broadband Spectra Generation** submitted by **MD SIZAN (213-33-1420) & Asibur Rahman (213-33-1451)** has been done under my supervision and accepted as satisfactory in partial fulfillment of the requirements for the degree of **Bachelor of Science in Electrical and Electronic Engineering** in **October, 2025.**

Signed

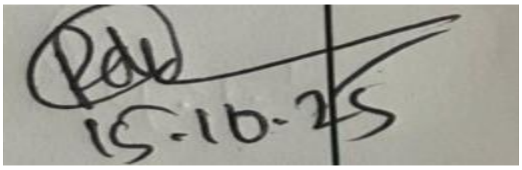

Dr. Mohammad Rezaul Karim
Professor,
Department of Electrical and Electronic Engineering
Faculty of Engineering
Daffodil International University

Dedicated

To

Our

Teachers & Parents

TABLE OF CONTENTS

LIST OF FIGURES	**viii-ix**
LIST OF ABBREVIATIONS	**x-xi**
LIST OF SYMBOLS	**xii-xiii**
ACKNOWLEDGMENT	**xiv**
ABSTRACT	**xv**
CHAPTER 1: INTRODUCTION	**1-6**
1.1 Introduction	1-3
1.2 Problem Statement	3-4
1.3 Objectives	4
1.4 Brief Methodology	5
1.5 Implementation Schedule (Gantt Chart)	5
1.6 Structure of the Report	6
CHAPTER 2: LITERATURE REVIEW	**7-10**
2.1 Introduction	7-8
2.2 Related Research	8-9
2.3 Compare and Contrast	9-10
2.4 Summary	10
CHAPTER 3: MATERIALS AND METHODS	**11-19**
3.1 Introduction	11
3.2 Methods and Materials	11-12
3.3 Design Specifications	12-13

3.4 Design Analysis	13-18
3.5 Simulation	18-19
3.6 Summary	19
CHAPTER 4: RESULTS AND DISCUSSIONS	**20-38**
4.1 Results	20-36
4.2 Discussions	36-38
CHAPTER 5: THESIS MANAGEMENT	**39-40**
5.1 Resources and Cost Management	39-40
5.2 Lesson Learned	40
CHAPTER 6: IMPACT ASSESSMENT OF THE THESIS	**41-44**
6.1 Economical, Societal and Global Impact	41-42
6.2 Environmental and Ethical Issues	42
6.3 Utilization of Existing Standards	43
6.4 Other Concerns	43-44
CHAPTER 7:CONCLUSIONS AND RECOMMENDATIONS	**45-48**
7.1 Conclusions	45-46
7.2 New Skills and Experiences Learned	47
7.3 Future Recommendations	47-48
REFERENCES	**49-52**
APPENDIX A: TURNITIN REPORT	**53-54**

APPENDIX B: COMPLEX ENGINEERING PROBLEM SOLVING AND ENGINEERING ACTIVITIES **55-56**

APPENDIX C: PROGRAM CODE **57-58**

LIST OF FIGURES

Figure No	*Figure Name*	*Page No.*
Fig. 1.1	A conventional optical fiber.	1
Fig. 1.2	Cross-section of the hexagonal Silica photonic crystal fiber showing geometry and simulation domain: solid core (d_1), air-hole diameter (d_2), pitch (Λ), air-hole lattice, and the absorbing boundary (PML).	2
Fig. 3.1	Finite-element discretization of the PCF cross-section.	13
Fig. 3.2	Finite-difference slopes: forward, backward, and centered derivative approximations x.	15
Fig. 3.3	Split-Step Fourier Method Spectral broadening hematic—alternating dispersion-only and nonlinearity-only sub-steps.	16
Fig. 4.1	Spectral broadening hematic cross-sections of the three-ring hexagonal PCFs in silica with air-hole	20
Fig. 4.2	Spectral broadening hematic cross-sections of the five-ring hexagonal PCFs in silica with air-hole	21
Fig. 4.3	Dispersion $D(\lambda)$ versus wavelength for a three-ring PCF ($\Lambda = 2.0\ \mu m$) with $\frac{d}{\Lambda} = 0.6, 0.7, 0.8$	23
Fig. 4.4	Dispersion $D(\lambda)$ versus wavelength for a five-ring PCF ($\Lambda = 2.0\ \mu m$) with $\frac{d}{\Lambda} = 0.6, 0.7, 0.8$	23
Fig. 4.5	Confinement loss versus wavelength for a three-ring PCF ($\Lambda = 2.0\ \mu m$), $\frac{d}{\Lambda} = 0.6, 0.7, 0.8$	25

Fig. 4.6	Confinement loss versus wavelength for a five-ring PCF ($\Lambda = 2.0\,\mu m$), $\frac{d}{\Lambda} = 0.6, 0.7, 0.8$	25
Fig. 4.7	$A_{eff}(\lambda)$ for the three-ring PCF ($\Lambda = 2.0\,\mu m$), $\frac{d}{\Lambda} = 0.6, 0.7, 0.8$	26
Fig. 4.8	$A_{eff}(\lambda)$ for the five-ring PCF ($\Lambda = 2.0\,\mu m$), $\frac{d}{\Lambda} = 0.6, 0.7, 0.8$	27
Fig. 4.9	$\gamma(\lambda)$ for the three-ring PCF ($\Lambda = 2.0\,\mu m$), $\frac{d}{\Lambda} = 0.6, 0.7, 0.8$	28
Fig. 4.10	$\gamma(\lambda)$ for the five-ring PCF ($\Lambda = 2.0\,\mu m$), $\frac{d}{\Lambda} = 0.6, 0.7, 0.8$	29
Fig. 4.11	Nonlinear evolution in 3-Ring SilicaPCF ($\Lambda = 2.0$ μm; $\frac{d}{\Lambda} = \{0.6,0.7,0.8\}$; $\lambda_{\mathrm{p}} = 1.2$ μm; P_0=30 kW).	32
Fig. 4.12	Output spectra at the fiber end for 3-Ring Silica PCF ($\Lambda = 2.0$ μm; $\frac{d}{\Lambda} = \{0.6,0.7,0.8\}$; $\lambda_{\mathrm{p}} = 1.2$ μm; $P_0 = 30\ kW$).	33
Fig. 4.13	Nonlinear evolution in 5-Ring Silica PCF ($\Lambda = 2.0$ μm; $\frac{d}{\Lambda} = \{0.6,0.7,0.8\}$; $\lambda_{\mathrm{p}} = 1.2$ μm; P_0=30 kW).	34
Fig. 4.14	Output spectra at the fiber end for 5-Ring Silica PCF ($\Lambda = 2.0$ μm; $\frac{d}{\Lambda} = \{0.6,0.7,0.8\}$; $\lambda_{\mathrm{p}} = 1.2$ μm; $P_0 = 30\ kW$).	35

LIST OF ABBREVIATIONS

FEM	Finite Element Method
FFT	Fast Fourier Transform
FWM	Four-Wave Mixing
FDM	Finite-Difference Method
GNLSE	Generalized Nonlinear Schrödinger Equation
GVD	Group Velocity Dispersion
MI	Modulation Instability
MI-SC	Modulation Instability–Supercontinuum
MIR	Mid-Infrared Region
NLSE	Nonlinear Schrödinger Equation
PBG	Photonic Bandgap Fiber
PCF	Photonic Crystal Fiber
PMC	Perfect Magnetic Conductor
PML	Perfectly Matched Layer
RK	Runge–Kutta Method
SBS	Stimulated Brillouin Scattering
SC	Supercontinuum
SPM	Self-Phase Modulation
SRS	Stimulated Raman Scattering
SSFM	Split-Step Fourier Method
ZDW	Zero Dispersion Wavelength

HOD	Higher-Order Dispersion
CW	Continuous Wave
OCT	Optical Coherence Tomography
OSF	Optical Signal Fidelity
TIR	Total Internal Reflection

LIST OF SYMBOLS

Symbol	Name of the symbol
Λ	Pitch of the photonic crystal fiber (PCF)
d	Diameter of the air holes
β	Propagation constant
ω	Angular frequency
v_g	Group velocity
c	Speed of light in vacuum
n_g	Group refractive index
L^D	Dispersion length
T_0	Pulse width
D	Dispersion parameter
χ	Electric susceptibility
ε_0	Vacuum permittivity
n^L	Linear refractive index
n_2	Nonlinear refractive index
γ	Nonlinear coefficient
λ	Operating wavelength
$A_{e}ff$	Effective mode area
L^{NL}	Nonlinear length
$L_{e}ff$	Effective length
φ^{NL}	Nonlinear phase shift
k_0	Free-space wavenumber ($2\pi/\lambda$)

L_W	Walk-off distance
E	Electric field
g^R	Raman gain factor
f^R	Raman fractional factor
N	Soliton order
P_0	Pulse peak power
A	Electric field amplitude
H	Magnetic field
μ_0	Vacuum permeability
n_{eff}	Effective refractive index
L_c	Confinement loss
α	Attenuation constant

ACKNOWLEDGEMENT

First of all, we want to give thanks to **Almighty Allah**. With his blessing we are able to complete our work with best effort.

We want to pay our utmost respect to our Supervisor **Dr. Mohammad Rezaul Karim, Professor** of the **Department of EEE, Daffodil International University** for who has given us the chance to work on an impactful idea and taken care of every issue of development of this concept. Then we would like to take this opportunity to express gratitude to our supervisor for being dedicated in supporting, motivating and guiding us throughout this project. This project can't be done without his useful advice and help. Also thank him very much for giving us the opportunity to work with this project.

We also want to convey our thankfulness to **all respected teachers** of the **Department of EEE, Daffodil International University** for their support and encouragement. Apart from that, we would like to thank our entire class fellows for sharing knowledge; information and helping us in making this project a success. To our beloved family, we want to give them our deepest love and gratitude for being very supportive and also for their inspiration and encouragement during our studies in this Institution.

ABSTRACT

This thesis investigates Spectral broadening in index-guiding silica photonic crystal fibers (PCFs) designed for all-anomalous dispersion at a 1.2 µm pump (30 kW). Two hexagonal lattices are compared—a 3-Ring and a 5-Ring cladding—with pitch Λ = 2 µm and air-fill ratios d/Λ= 0.6, 0.7, 0.8. Linear properties—chromatic dispersion $D(\lambda)$, effective mode area $A_{\mathrm{eff}}(\lambda)$, nonlinear coefficient $\gamma(\lambda)$, and confinement loss—are extracted using full-vector finite-element eigenmode analysis with perfectly matched Rings. These wavelength-dependent parameters feed a Generalized Nonlinear Schrödinger Equation (GNLSE) solver to predict three outputs: spectral power vs wavelength, distance vs temporal delay, and distance vs wavelength evolution. Both fibers place the pump in the anomalous regime, but they differ markedly in long-wave performance. The 3-Ring design exhibits slightly stronger anomalous curvature near 1.2 µm yet suffers orders-of-magnitude higher confinement loss beyond ≈2.5 µm, leading to early decay of red-shifted components. The 5-Ring design delivers flatter anomalous dispersion, smaller A_{eff} and hence higher γat the pump, and—critically—much lower long-wave leakage, preserving energy transport toward 3 µm. Nonlinear propagation maps confirm smoother soliton dynamics, robust dispersive-wave generation, and broader, more uniform spectra for the 5-Ring fiber. Across both designs, increasing d/Λ reduces A_{eff} and raises γ; the combination $d/\Lambda \approx$ 0.7–0.8 in the 5-Ring geometry is recommended as the optimized design. The 3-Ring fiber is retained as a comparative baseline to highlight improvements in dispersion flattening and long-wavelength guidance.

Keywords: Photonic Crystal Fiber; Anomalous Dispersion; Confinement Loss; Effective Mode Area; Nonlinear Coefficient; Finite-Element Method; Generalized Nonlinear Schrödinger Equation.

Chapter 1

Introduction

1.1 Introduction

Optical Fibers, indispensable in today's telecommunication systems, have developed during the years in order to support high-capacity data transmission. The last two decades has seen much progress in the field of fiber optics with the introduction of PCFs which possess properties not exhibited by conventional fibers. Unlike standard fibers that guide light through total internal reflection, PCFs use a microstructured cladding (composed of an array of air holes in most general cases) which allow them to also guide the light by index-guiding as well as photonic bandgap. Such flexibility enables tailoring of several optical parameters such as dispersion, confinement loss, and effective mode area, thereby rendering PCFs highly versatile for widespread applications [1, 2, 3, 4].

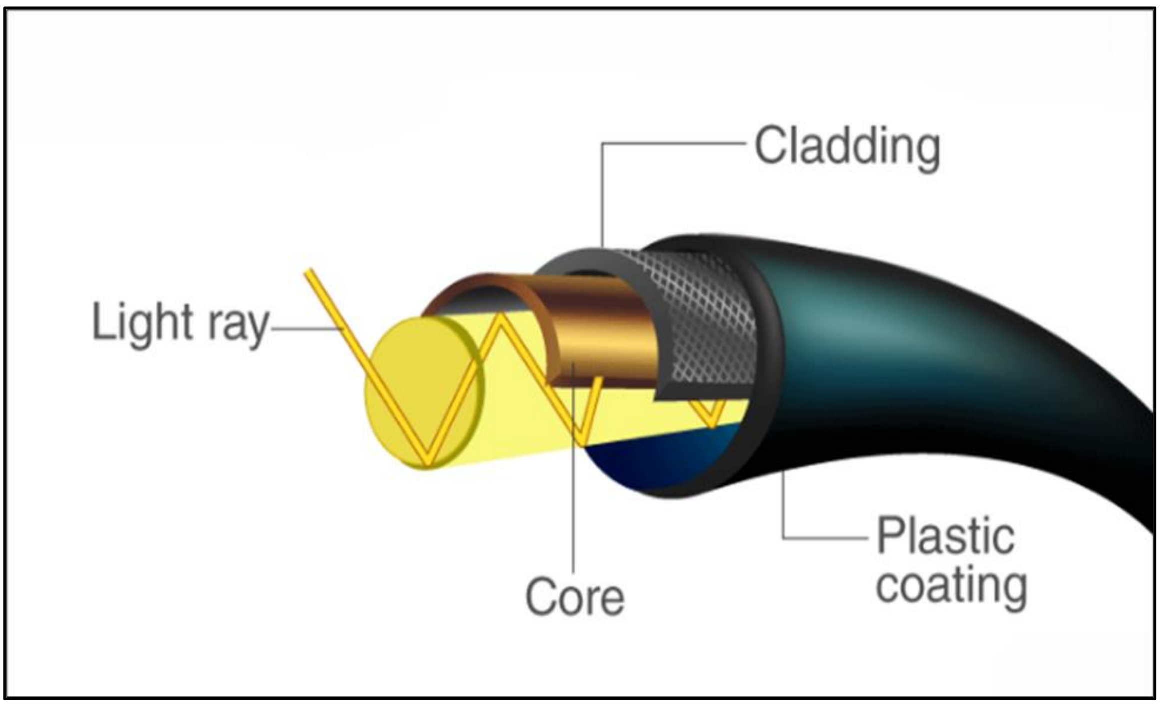

Figure 1.1: A conventional optical fiber

A notable application where PCFs can be used for various sensing application. Due to nonlinear interactions in the fiber and produce very wide optical spectra. These spectra are required in many modern devices, such as Optical Coherence Tomography (OCT), spectroscopy, biomedical imaging and detection of hazardous materials. It is the possibility of control over both linear and nonlinear properties in PCFs that makes them attractive, because it allows generation of high-power/efficiency broadband spectra [1] [3] [5].

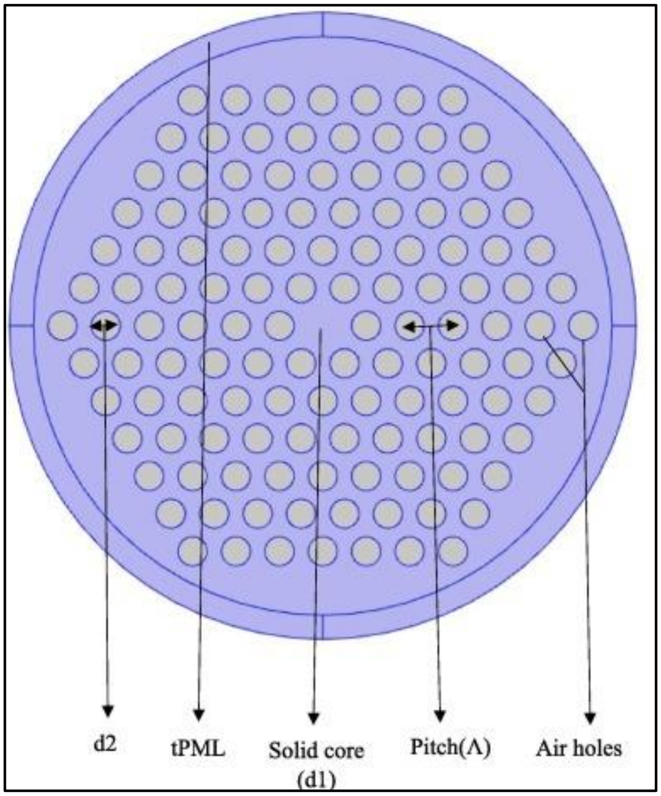

Figure 1.2: Cross-section of the hexagonal Silica photonic crystal fiber showing geometry and simulation domain: solid core (d_1), air-hole diameter (d_2), pitch (Λ), air-hole lattice, and the absorbing boundary (PML)

- Air-hole diameter (d): The diameter of each circular air void in the cladding. Increasing d (or the ratio d/Λ) raises index contrast, generally pushing the dispersion more negative, shrinking the effective mode area A_{eff}, and increasing nonlinear coefficient γ; excessively large d can, however, increase confinement loss and fabrication sensitivity [6].
- Pitch (Λ): Center-to-center spacing between adjacent air holes. Smaller Λ tightens confinement and reduces A_{eff} (larger nonlinear γ), but also shifts the dispersion and can

move zero-dispersion wavelengths; too small Λ may raise Spectral broadening attering loss.

- ❖ Core: Formed by omitting the central air hole(s). Its diameter sets the fundamental mode size and strongly influences A_{eff} and the sign of group-velocity dispersion (GVD) near the pump.
- ❖ Cladding: The hexagonal lattice of air holes surrounding the core. Its number of rings (e.g., 3-Ring vs 5-Ring) governs leakage: more rings usually lower confinement loss and slightly modify dispersion via the space-filling mode of the lattice.
- ❖ PML: An annular, non-physical region used only in numerical models to absorb outgoing fields and measure leakage; its thickness is tuned to prevent spurious reflections.

In the spectral broadening, PCFs have a distinctive advantage compared to conventional fibers as their dispersion profiles can be specifically tailored to promote nonlinear interactions. For instance, because all-anomalous dispersive PCFs can sustain spectral broadening over wider bandwidths including mid-infrared (MIR) band. For that reason, the capability to tailor fibers to manage both optimized dispersion and Kerr effects is essential to improve on spectral broadening generation, a fact that leads Polarization-maintaining PCFs as good candidates for next decades light sources [1] [4] [7].

In this work, we specifically concentrate on the design and investigation of multi-Ring Silica PCFs with all-anomalous dispersion profile to tailor it for broadband spectral broadening generation. Through changes in fiber structure, including air-hole diameter, pitch and a number of rings, this work is attempting to optimize spectral broadening especially between $0.5 - 3.0\,\mu m$ wavelengths. The aim is to develop fibers showing efficient Beam Waveguide including in the MIR spectral windows, which find increasing interest for various applications in spectroscopy and medical diagnostics.

1.2 Problem Statement

Traditional optical fibers, especially the silica-based ones, when they are used have a limited performance in terms of broadband spectra with wide spectral coverage particularly in the longer wavelength MIR region. The inherent limitations of the same lie in their limited design flexibility, with a poor control over dispersion and nonlinear properties. Although PCFs afford for additional degrees of freedom in designing the fiber structure, the problem is how to tailor the fiber geometry so as to simultaneously optimize spectral broadening over a wide range of wavelengths. Notably, PCFs with all-anomalous dispersion have produced good prospectivities for the spectral broadening, but still little is known on how to correct geometric parameters for broadband generation around pump wavelengths such as 3.0 μm [3].

The geometrical parameters, such as air-hole diameter, pitch size and the number of cladding rings can impact significantly on important fiber properties, for instance confinement loss, effective mode area (A_{eff}), nonlinear coefficients, γ of fiber and also its dispersion behavior. It is necessary to maximize these parameters for reasonable generation and low loss spectral broadening. To fill in the gap in the existing literature, this work thoroughly studies these parameters from a systematic point of view and optimizes the PCF structure for broadband spectra generation [1].

1.3 Objectives

The major purposes of this investigation are:

- To study the influence of different geometric parameters on the dispersion optimization nonlinear multi-ring silica PCFs.
- To find the optimum PCF structure (air-hole diameter, pitch, and the number of cladding rings) for efficient broadband spectra generation, especially in the MIR region.
- To realize a PCF structure with low confinement loss, high nonlinearity and specific dispersion profiles for broad spectra.
- To model generation of the supercontinuum as a function of the pump power and wavelength, and analyze the spectra obtained.

1.4 Brief Methodology

The approach is based on numerical simulations to study and optimize multi-ring PCFs for spectral broadening. The approach includes:

- ❖ **Geometrical design & analysis Performed by Finite Element Method (FEM) based COMSOL Multiphysics:** PCF designs are made by changing the air-hole diameter, pitch and number of rings. These parameters are varied to investigate their effect on dispersion, confinement loss and effective area.
- ❖ **Nonlinear pulse propagation simulation:** The GNLSE is solved by MATLAB in order to spectra generation process.

1.5 Implementation Schedule (Gantt Chart)

Phase / Task	1–2 Month	3–4 Month	5–6 Month	7–8 Month	9–10 Month	11–12 Month
Phase 1: Design & Simulation Phase						
Literature Review	✓	✓				
Theoretical Study (Optics, Dispersion, SCG)		✓	✓			
Structure Design (Multi-Ring Silica PCF)			✓	✓		
Parameter Optimization (d, Λ, core size)			✓	✓		
Simulation & Validation (FEM/PML Model)				✓	✓	
Phase 2: Analysis & Documentation Phase						
Spectral Analysis (Broadband Generation)				✓	✓	
Data Interpretation & Result Discussion					✓	
Report Writing (Draft & Revision)					✓	✓
Final Editing & Formatting						✓
Defense Preparation (Presentation & Submission)						✓

1.6 Structure of the Report

The rest of this report is organized as follows:

- ❖ Chapters 1: Introduction - Introduction to problem, aims of the research, methods and lip structure of the thesis.
- ❖ Chapter 2: Literature Review - Examination of previous work on photonic crystal fibers, supercontinuum (SC) generation and related works.
- ❖ Chapter 3: Methods and Materials - Detailed description of design, simulation and optimization methods for Suspended Core Fiber (SCF).
- ❖ Chapter 4: Results and Discussions - Presentation testing and discussion of numerical simulations results.
- ❖ Chapter 5: Thesis Management - Presents the work plan (tasks, schedule, milestones), resources (FEM/SSFM toolchain), and risk controls (mesh/step-size convergence, energy conservation, cross-checks).
- ❖ Chapter 6: Impact Assessment of the Thesis - Assesses economic, societal, and environmental benefits of a silica-based SC source (lower cost/complexity than exotic glasses; OCT/spectroscopy/sensing potential), and references safety/standards considerations
- ❖ Chapter 7: Conclusion and Future - Work Summary and future prospects of findings.

Chapter 2

Literature Review

2.1 Introduction

PCFs have been a rapidly progressing research area for the past few decades due to their capability of offering control over both linear and nonlinear optical properties. PCFs are nothing but optical fibers with a microstructured array of air holes in its length, resulting them to have distinct above others properties than conventional ones. Unlike conventional fibers, which rely upon Total Internal Reflection (TIR) to confine light, PCFs allows a combination of index-guiding and Photonic Band Gap (PBG) guiding mechanisms to guide the light, and can be designed with more flexibility.

Due to their microstructure cladding as well as the flexibility of engineering geometrical parameters such as air-hole diameter, lattice pitch and number of rings, PCFs can be designed to offer customized dispersion, low confinement loss and high nonlinearity. These properties make PCFs very flexible, and they can be applied to numerous applications in telecommunications, medical imaging, spectroscopy and structural sensing. One of the most fainting phenomena exhibited by PCFs is that of Spectral broadening , where a narrow-band pulse of light undergoes dramatic spectral broadening to give nearly white light [5] [4].

Control over spectral broadening generation is indispensable for several applications, such as OCT, frequency metrology and spectroscopy. As a result, this effect has attracted much interest for MIR applications in which the broadband nature of light is critical for sensing and imaging. Due to the possibility of controlling dispersion and nonlinearity of light, PCFs are suitable for increasing spectral broadening efficiency and improving broadband sources.

In this chapter we will summarize the main developments in PCF research, and particularly their design parameters as applied to the spectral broadening process, as well as the influence of different geometrical modifications on the optical properties of these fibers. We will also examine the physical behavior responsible for spectral broadening and review experimental and numerical works in this field.

2.2 Related Research

Many researches have been performed to design and optimize the PCFs for spectral broadening. One of the earliest papers which looked at SC generation in PCFs was by Ranka et al. in 2000. They presented ultrabroadband SC generation across an octave with a photonic crystal fiber [8]. Their work demonstrated the significance of dispersion engineering and nonlinear interactions for generating SC, that paved way for the number of further investigations on PCF based SC generation.

A significant advance was made in studies of Dudley et al. submitted a thorough overview of SC generation in PCFs in 2006, focusing particularly on the nonlinear propagation leading to pulse shaping. A detailed investigation of the temporal and spectral properties of the supercontinuum generation including its underlying mechanisms (SPM, FWM, soliton fission and DWGs) was covered in their review. This work is of significance in the studies of producing SC in that it furnished theoretical and experimental information for SC generation, illuminating the dominant position femtosecond pulse played during the course of SC generation, especially on the anomalous dispersion region of PCFs [4].

Furthermore, Genty et al. (2002) and Herrmann et al. (2002) investigated the soliton dynamics for SC generation with a special emphasis on the effect of soliton fission. Soliton fission takes place when a soliton decomposes into several lower-energy ones, every one of them generating some extra frequencies. We demonstrated this process to be essential when generating SC in the femtosecond regime, i.e., high peak powers and short pulse durations [8].

Apart from soliton dynamics, the fiber geometry and material properties also have a large impact on the efficiency of SC. For example, Biswas et al. (2015) studied the influence of air-hole diameter and lattice pitch on a hexagonal PCF's optical properties [9]. They found that the larger air-hole size and the smaller lattice constant could drastically reduce confinement loss but increase nonlinearity interaction, which were favorable for improving SC power conversion efficiency. They have also shown that the pitch to diameter ratio is an important parameter in dispersion management affecting directly the both confinement loss and effective index.

The fiber type is also an important factor affecting the generation of SC. Although silica is the most popular material for PCFs, chalcogenide glasses (e.g., GeAsSe glass) have recently been investigated to achieve SC generation in the mid-IR range. Karim et al. (2015) reported SC generation from $1.7\ to\ 18\ \mu m$ in GeAsSe chalcogenide PCFs, when pumped at $3.1\ \mu m$ with a $4000\ W$ peak power and pulse length of $50\ fs$. This paper demonstrates the promise of high nonlinear refractive index material-based PCFs for producing MI-SC , which is extremely important for medical diagnostics and spectroscopic applications.

Computer simulations have also been widely employed to simulate SC generation in PCFs. For example, Liu et al. (2001)) applied a GNLSE in order to describe the phenomenon of SC generation on a tapered PCF [8]. Their numerical simulations indicate that higher-order dispersion and stimulated Raman Spectral broadening attering are some of the most important effects causing spectral broadening for femtosecond pump pulses, pitch optimization also has an important impact on improvement of spectral width.

In addition to femtosecond pulses, several works have also reported excited SC generation using longer pulse widths and Continuous Wave (CW) sources in PCFs. Studies by Golovchenko et al. (1991) and Provino et al. (2001) showed that even in the case of longer FWHM pulses or CW pumping, for which broadening is due to four waves mixing (FWM) combined with Raman Spectral broadening attering, soliton dynamics play an important role in SC generation.

2.3 Compare and Contrast

By examining 3-Ring to 5-Ring hexagonal PCFs, strong differences can be observed. In a 5-Ring PCF, better dispersion control was induced, and the obtained SC spectrum is broader. This arises from the larger geometrical complexity for a 5-Ring design and then the improved dispersion management capability. Leave aside the 3-Ring PCFs are easier to experiment and lower in confinement loss, and thus can be used more in low-loss-required applications [6].

Also, air-hole diameter and lattice constants are important in the optimization of nonlinear interactions in PCFs. The larger air hole diameters yield higher nonlinear coefficients (γ), leading to more efficient SC generation. But a large diameter is likely to make the confinement loss arc higher, that should be carefully controlled. Smaller lattice pitches, on the other hand, could lead to better dispersion but may worsen confinement loss demanding careful optimization of design [10].

2.4 Summary

PCF design for SC generation is an elegant dance of dispersion, confinement loss, effective area and nonlinearity. Geometrical parameters (e.g., air-hole diameter, lattice pitch) and material properties have been shown to play a key role in modifying the optical behavior of such a fiber from different point of view. Although 5-Ring PCFs represent more advanced dispersion control for broadband SC generations, using free 3-Ring PCFs is still interesting due to the lower confinement loss [11].

These latest developments involving numerical calculation, especially based on the GNLSE have proved to be very helpful for understanding the nonlinear description of SC generation in PCFs. The new class of advanced fiber designs and use of nonlinear materials, such as chalcogenide glasses, has enabled a renaissance in mid-infrared SC generation that holds great promise for medical imaging, spectroscopy, and frequency metrology applications [12] [13].

Chapter 3

Materials and Methods

3.1 Introduction

This chapter describes the computational framework used to extract the linear properties—chromatic dispersion $D(\lambda)$, confinement loss $L_c(\lambda)$, and effective mode area $A_{eff}(\lambda)$ −and simulate the nonlinear pulse propagation that leads to SC generation in the proposed multi-Ring PCFs [22][28].

Two PCFs families are treated: a 3-Ring and a 5-Ring hexagonal lattice. Unless otherwise stated, the cladding holes are air-filled, the base material is fused silica, the pump is centered at $1.2\ \mu m$, and the target spectral broadening span is $0.5 - 3.0\ \mu m$.

The workflow is organized as follows:

- ❖ Cross-sectional eigen analysis (FEM/FDM) → $n_{eff}(\lambda)$, modes, fields $(x, y), H(x, y)$, A_{eff}, L_c.
- ❖ Differentiation of $\beta(\omega) = n_{eff}(\lambda)\,\omega/c \rightarrow\ \beta_k\ and\ D(\lambda)$.
- ❖ Nonlinear parameters from modal fields → $\gamma(\lambda)$.
- ❖ Time-domain propagation Split-Step Fourier Method/Runge–Kutta Method (SSFM/RK) of the GNLSE with Raman/self-steepening to generate spectra, spectrograms, and evolution maps.

3.2 Methods and Materials

The fiber host is fused silica; air fills all cladding holes. The wavelength-dependent refractive index $n(\lambda)$is evaluated from the Sellmeier form appropriate for silica. Where explicit coefficients are required in calculations or plots, standard three-term Sellmeier parameters for fused silica are used. Material loss of silica is neglected in the 0.5–3.0 μm band except where noted [1].

Two hexagonal lattices are considered:

- 3-Ring PCF: three rings of air holes around a solid core.
- 5-Ring PCF: five rings (baseline for optimization).

Both families are parameterized by pitch $\Lambda = 2\,\mu$m and relative hole size $d/\Lambda \in \{0.6, 0.7, 0.8\}$. The core is formed by omitting the central hole (index guiding). The 5-Ring variant increases modal confinement and suppresses leakage at long wavelengths, a known advantage of adding rings in hexagonal PCFs.

Software and solvers. Linear modal analysis is performed with a finite-element (FEM) eigenmode solver using triangular meshes and perfectly matched Rings (PMLs) to absorb outgoing fields, from which $n_{\text{eff}}(\lambda)$and loss are extracted. Comparable FEM-PML configurations are standard in PCF design practice for accurate dispersion and leakage predictions [15] [16].

Nonlinear propagation is carried out in MATLAB using a SSFM integration of the GNLSE with Raman response and Higher-Order Dispersion (HOD). Similar SSFM implementations are used throughout the spectral broadening literature [1] [15].

3.3 Design Specifications

Operating band and pump. The target SC spans 0.5–3.0 μm. Pumping is at 1.2 μm (peak power 30 kW) in the anomalous regime of both designs to favor soliton dynamics and dispersive-wave generation into the short-wavelength edge.

Dispersion objective. All-anomalous operation from the pump toward the long-wavelength edge is enforced; Zero-Dispersion Wavelength(s) (ZDW) must lie below 1.2 μm. The 5-Ring design is tuned for a flatter $D(\lambda)$profile to support phase-matched energy transfer across the band with reduced walk-off, consistent with prior optimization strategies in hexagonal PCFs [1] [10].

Confinement and manufacturability. Confinement loss below ~10^{-3} dB/m is targeted up to 3 µm. Increasing ring count is a pragmatic route to suppress leakage without strongly perturbing dispersion—hence the preference for 5 Rings for the final design. Practical tolerances on $d$and $\Lambda$are set by stack-and-draw feasibility; fewer rings (3-Ring) simplify fabrication but raise long-wave leakage risk, as corroborated by prior PCF comparisons.

3.4 Design Analysis

Obtain vectorial guided modes and their effective indices over wavelength for arbitrary PCF geometries; compute A_{eff}, L_c, and waveguide dispersion. A full-vector FEM is preferred for high-index-contrast holey structures and noncircular domains.

Governing equations and weak form. For longitudinally invariant structures, a vectorial $H-$field formulation is discretized by Galerkin FEM on triangular elements (quadratic nodal basis). The resulting sparse generalized eigenproblem returns n_{eff} and transverse fields (Hx, Hy) for each mode. Material dispersion is included explicitly via a Sellmeier model for silica [23].

Effective area. From the transverse mode distribution $F(x, y)$ (normalized field envelope).

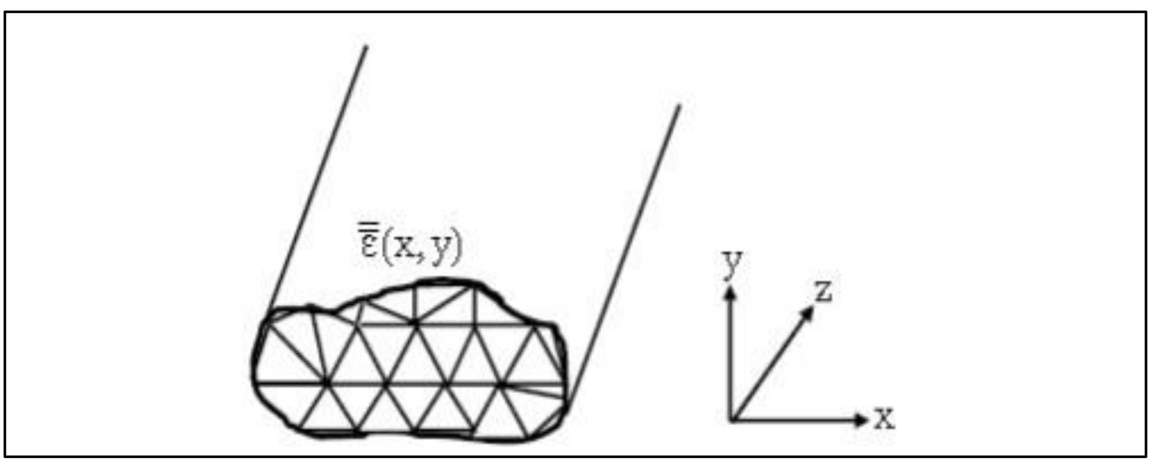

Fig 3.1: Finite-element discretization of the PCF cross-section

$$A_{eff}(\lambda) = \frac{\left(\iint |F|^2 dx\, dy\right)^2}{\iint |F|^4 dx\, dy} \tag{4.1}$$

which we compute on the FEM mesh at each λ.

Confinement loss. With complex $n_{eff} = n' + i\, n''$ (from leaky boundary treatment), the attenuation is

$$L_c(\lambda) = 8.686 \times 2k_0 Im\left(n_{eff}\right) \tag{4.2}$$

Dispersion from $n_{eff}(\lambda)$. We evaluate $\beta(\omega) = n_{eff}(\lambda)\, \omega/c$ and compute numerical derivatives $\beta_k = \frac{d^k\beta}{d\omega^k}|_{\omega_0}$. The dispersion parameter $(ps\ /\ nm\ km)$ follows

$$D(\lambda) = -\frac{2\pi c}{\lambda^2}\beta_2(\lambda) \tag{4.3}$$

Equivalently, using finite differences on $Re[n_{eff}]$ vs λ yields the same D (units conversion accounted), and is common in FEM workflows.

Meshing and convergence.

- Minimum $8 - 12$ elements across the smallest air-hole diameter and ≥ 4 elements across struts between holes.
- Curved-boundary refinement for hole perimeters; growth rate ≤1.3 from core to outer cladding.
- Convergence is declared when n_{eff} changes by $< 10^{-6}$ and $A_{eff}$by $< 0.5\%$ under global mesh refinement and PML-thickness variation.

Parameter sweeps, To study geometry effects (hole diameter d, pitch Λ, number of rings), we sweep $d/\Lambda \in$ [0.35,0.7] and $\Lambda \in$ [1.2,2.6] μm for both 3- and 5-Ring lattices; at each point we extract $\{D,\ A_{eff}, \gamma, L_c\}$ across $0.5 - 3.0\ \mu m$.

Provide a second, independent check on modal trends and dispersion for selected geometries, using a Spectral broadening alar Helmholtz discretization on a Cartesian grid (useful for quick Spans), and to prototype absorbing boundary behavior before full FEM runs.

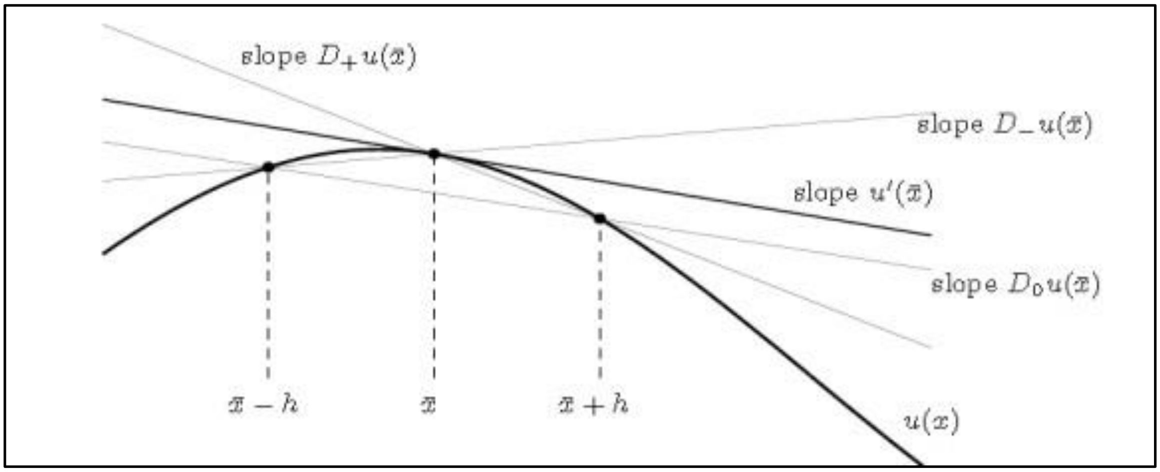

Fig 3.2: Finite-difference slopes: forward, backward, and centered derivative approximations x.

The Spectral broadening alar wave equation $\nabla^2 \perp \psi + k_0^2(x,y)\psi = \beta^2\psi$ is discretized with central differences on a Yee-style grid. Eigen pairs yield approximate n_{eff} maps; $D(\lambda)$ is obtained as in FEM via finite differences. FDM grids are padded with absorbing Rings (discrete PML or stretched-coordinate damping) to emulate open boundaries [23].

While vectorial effects are essential in final results (FEM), FDM is useful for: (i) sensitivity scans over $d/\Lambda, \Lambda$; (ii) quick checks of ZDW trends; (iii) validating PML thickness. Results are not used directly for γ or L_c.

deriving both Spectral broadening alar and full-vector variational formulations and casting the mode computation as a generalized eigenvalue problem $A\{x\} = \lambda B\{x\}$. It argues that the full-vector **H**-field formulation is preferable for anisotropic or inhomogeneous guides and explains how natural boundary conditions help avoid spurious solutions. Implementation details include triangular elements with appropriate shape functions, assembly of global matrices, and adaptive mesh refinement concentrated near high-field regions [27].

High-accuracy integration of the nonlinear step inside the split-step algorithm and, where needed, direct time-domain tests of stiff terms (e.g., Raman response).

In the enhanced SSFM used here, the nonlinear sub-step is integrated by a second-order Runge–Kutta (Heun) or fourth-order RK when testing accuracy, treating the self-steepening/Raman convolution explicitly as perturbations—an approach adopted in standard SCG modeling [4].

Simulate femtosecond–picosecond pulse propagation and SCG under the generalized nonlinear Spectral broadening hrödinger equation (GNLSE) with higher-order dispersion, Kerr effects, Raman response, and self-steepening. This method underpins nearly all SCG modeling and diagnostics (spectra, spectrograms, wavelength- and time-resolved evolution)

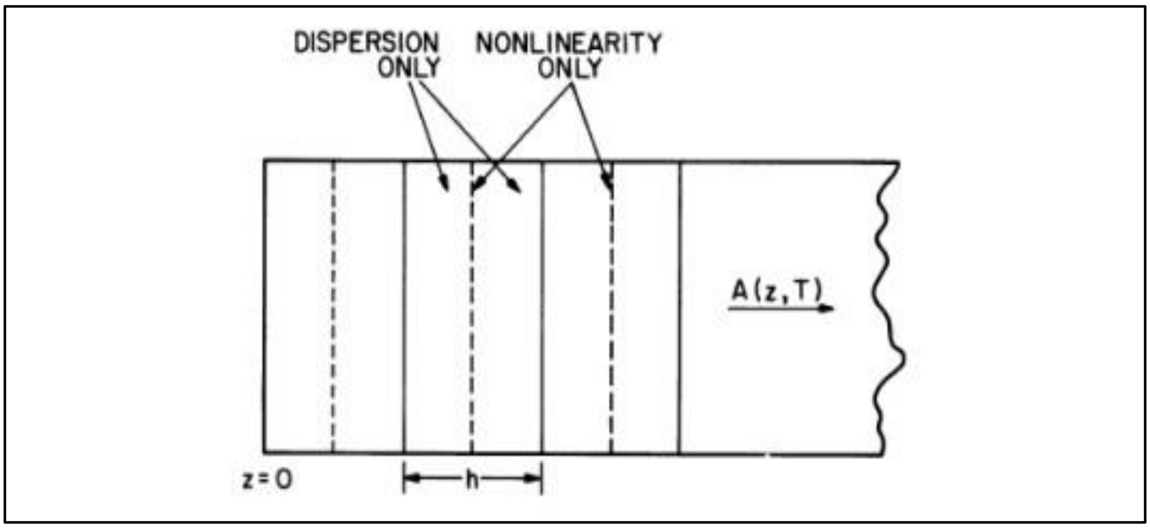

Fig 3.3: Split-Step Fourier Method Spectral broadening hematic—alternating dispersion-only and nonlinearity-only sub-steps.

In a frame moving at v_g, the complex envelope $A(z,T)$:

$$\frac{\partial A}{\partial z}+\sum_{k\geq 2}\frac{i^{k+1}}{k!}\beta_k\frac{\partial^k A}{\partial T^k}$$
$$=i\gamma(\omega_0)\left(1+i\tau_{shock}\frac{\partial}{\partial T}\right)\left[A(z,T)\int_{-\infty}^{\infty}R(\tau)|A(z,T-\tau)|^2 d\tau\right]+iT_R(z,T) \qquad (4.4)$$

where $R(\tau) = (1 - f_R)\delta(\tau) + f_R h_R(\tau)$ splits instantaneous and delayed Raman contributions, $\tau_{shock} \approx 1/\omega_0$ corrected for frequency-dependent A_{eff} *and* T_R represents spontaneous Raman noise when included[29]..

Sampling and windows. Accurate SCG requires very wide spectral and temporal windows. Following best practice:

- Choose N (power of two) such that $T_{span}F_{span} = N$, with $F_{span} \gtrsim 1000\ THz$ for octave-class SPECTRAL BROADENING and $T_{span} \gtrsim 20\ ps$ to avoid wrap-around.
- Use an absorbing temporal window (taper) to monitor photon-number conservation and suppress cyclic aliasing.
- Verify convergence by halving Δz and doubling N; ensure spectral/temporal features change $< 1 - 2\%$.

Step size control. Δz is adapted to $\min\{L_D, L_{NL}\}/10$, with dispersion length $L_D = T_0^2/|\beta_2|$ and nonlinear length $L_{NL} = 1/(\gamma P_0)$, and further restricted near soliton fission or steepening.

Noise and coherence. One-photon-per-mode quantum noise and spontaneous Raman noise can be added to assess coherence (not used for “deterministic” design sweeps).

Diagnostics. Besides spectra $|A(\lambda)|^2$ we compute spectrograms (short-time Fourier transforms) to correlate temporal and spectral features through evolution.

Silica model. The wavelength-dependent refractive index of fused silica is modeled with a 3-term Sellmeier law:

$$n^2(\lambda) = 1 + \sum_{j=1}^{3} \frac{B_j \lambda^2}{\lambda^2 - C_j}$$

with the standard silica coefficients applied across the simulation band (values as reported in the literature and commonly used in PCF modeling). Where required, coefficients can be (re)fitted from tabulated data using robust variable-projection least squares to avoid degeneracy and ensure stability across UV/IR bands. This $n(\lambda)$ feeds both the material contribution to dispersion and the index map $n(x, y; \lambda)$ used by FEM/FDM [23] [24].

Open boundaries. To emulate an unbounded cladding, Perfectly Matched Rings (PMLs) are wrapped around the computational domain in both FEM and FDM. We use at least $0.5 - 1.0\,\Lambda$ PML thickness with polynomial or exponential attenuation profiles; PML parameters are tuned so that (i) the real part of n_{eff} is insensitive ($< 10^{-6}$) to PML changes, and (ii) the imaginary part converges (stable L_c) under joint mesh–PML refinement [25] [26].

Mode selection and symmetry. Fundamental HE_{11} like modes are selected by symmetry filters and overlap with a Gaussian seed. Spurious modes (PML-guided or ring modes) are discarded by field inspection and loss thresholds.

SSFM boundaries**.** In time-frequency, periodic Fast Fourier Transform (FFT) boundaries are used; temporal apodization prevents wrap-around contamination, and photon-number conservation is monitored over z.

3.5 Simulation

GNLSE and numerical Spectral broadening heme. Pulse evolution is computed by SSFM integration of the single-polarization GNLSE with linear operator $\sum_{\mathrm{k}\geq 2} \beta_k\, \partial_{\mathrm{T}}^{\mathrm{k}}/\mathrm{k}!$(dispersion up to the order needed for numerical stability) and a nonlinear operator comprising Kerr, self-steepening, and Raman response $\mathrm{R(t)} = (1 - \mathrm{f_R})\delta(\mathrm{t}) + \mathrm{f_R h_R(t)}$. This formulation is standard in fiber-based SCG and is used to assess the impact of HOD on spectral broadening.

Discretization and stability. Simulations use a temporal window wide enough to avoid wrap-around, with time steps chosen to resolve the shortest emerging features; longitudinal step sizes satisfy the usual SSFM stability and accuracy criteria. Prior SCG studies demonstrate that inclusion of sufficient HOD terms is necessary for spurious-free spectra; we retain HOD until convergence is observed (checked by comparing spectra when adding/removing the highest-order term).

Pump and boundary settings. The input is a transform-limited femtosecond pulse at 1.2 μm (peak power 30 kW). Raman parameters for silica and the shock term $1/\omega_0\ \partial_T$are included [Ref]. Fiber lengths are selected to reach saturation of broadening without excessive numerical noise (few centimeters to a few tens of centimeters, depending on design). Spectral power density at the output, spectral evolution vs. distance, and temporal evolution vs. distance are recorded.

Outputs. For each geometry (3-Ring and 5-Ring) and each d/Λset, we produce: (i) output spectrum, (ii) distance–wavelength evolution (spectrogram-like plot), and (iii) distance–temporal-delay evolution. These outputs mirror what has been reported for PCF SCG under anomalous-regime pumping.

3.6 Summary

We modeled silica hexagonal PCFs with $\Lambda = 2\ \mu$mand $d/\Lambda \in \{0.6,0.7,0.8\}$ using FEM-PML eigenmode analysis to extract D, A_{eff}, γ, and confinement loss, followed by SSFM-GNLSE propagation at 1.2 μm, $30\ kW$. The 3-Ring design is easier to fabricate and supports strong anomalous dispersion but suffers high long-wave leakage. The 5-Ring design (optimized) flattens dispersion and dramatically reduces confinement loss across 2.5–3.0 μm, enabling more robust, broadband SC generation —an outcome consistent with prior experience in hexagonal PCFs.

Chapter 4

Results and Discussions

4.1 Results

We study index-guiding PCFs formed by omitting the central air hole (solid Silica core) and arranging circular air holes on a hexagonal lattice of pitch Λ. The cladding is built from 3 or 5 concentric rings. Guidance is by modified total internal reflection; dispersion and confinement are co-engineered through $\Lambda, d/\Lambda$, and the number of rings. Unless otherwise stated, all holes are air-filled and the glass is fused silica.

A "conventional" design uses a single Λ and a uniform d/Λ across rings. The $3-layer$ device is simpler to fabricate and can provide stronger anomalous D near the pump, but suffers higher long-wave leakage. The 5-Ring device chiefly suppresses confinement loss at $2.5-3.0\ \mu m$ with little penalty to dispersion, providing more reliable long-wave guidance for practical spectral broadening [31].

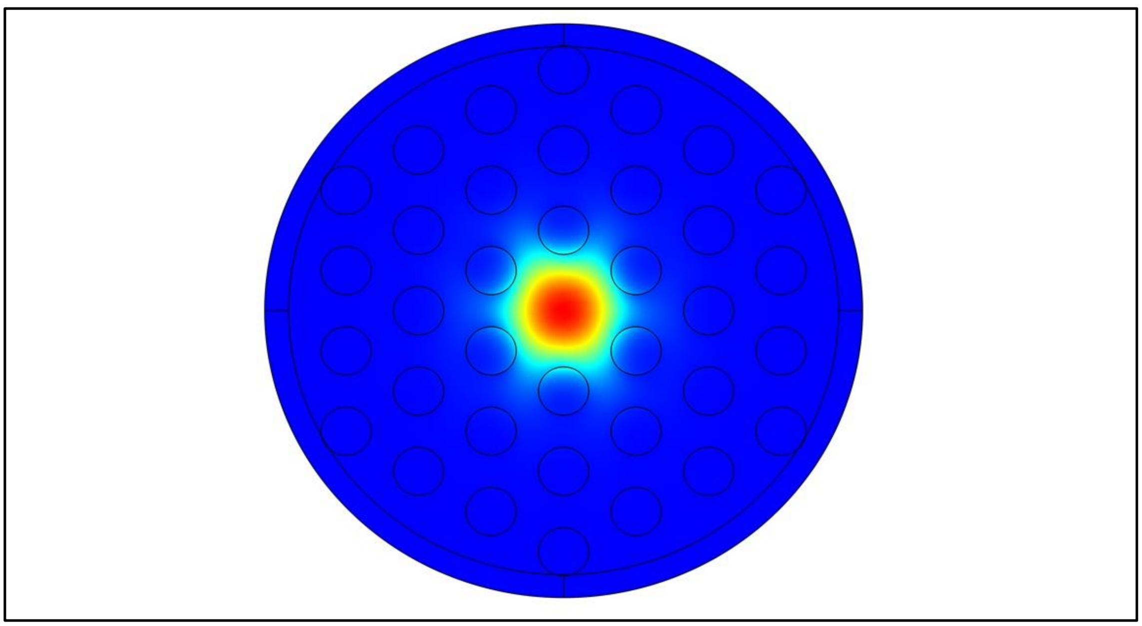

Figure 4.1: Spectral broadening hematic cross-sections of the three-ring hexagonal PCFs in silica with air-hole.

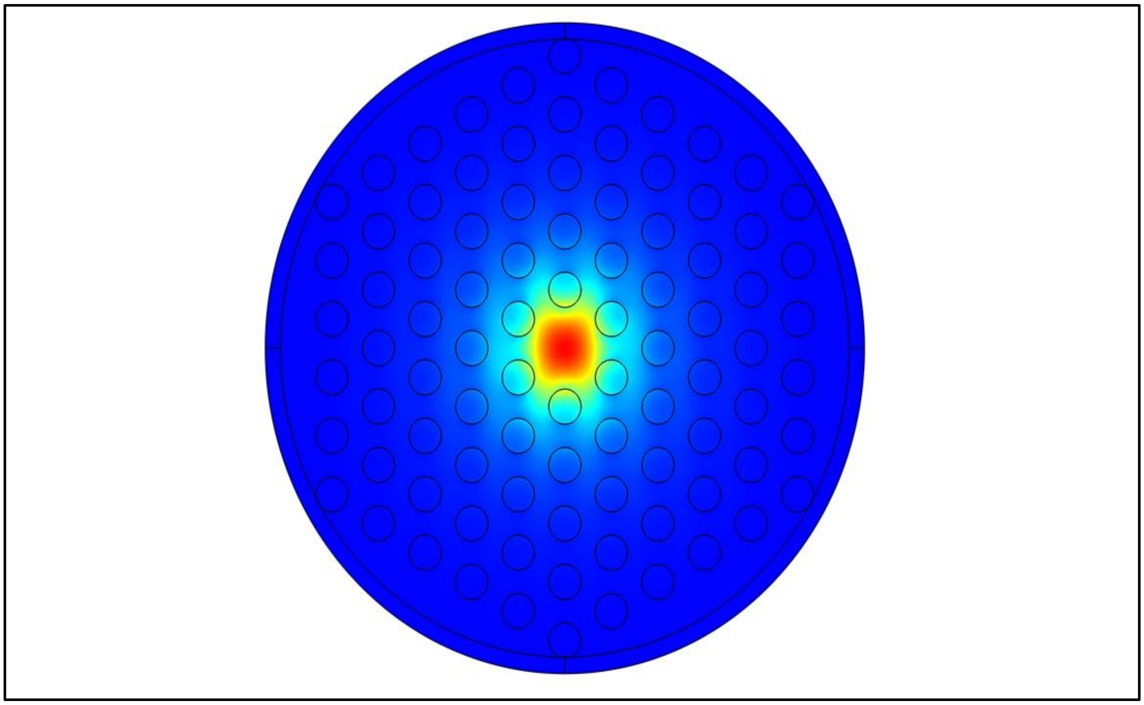

Figure 4.2: Spectral broadening hematic cross-sections of the five-ring hexagonal PCFs in silica with air-hole

Material dispersion $n(\lambda)$ is represented by a three-term Sellmeier law. Waveguide dispersion is taken from the fundamental-mode effective index $n_{eff}(\lambda)$ (full-vector eigenmodes). The quantities reported are computed as follows (consistent with standard fiber/PCF practice:

- $\mathrm{D}(\lambda) = -\frac{2\pi c}{\lambda^2}\beta_2(\lambda)$, where $\beta(\omega) = n_{eff}(\lambda)\omega/c$ and $\beta_2 = \frac{\partial^2\beta}{\partial\omega^2}$
- $A_{eff}(\lambda) = \frac{\left(\iint |F|^2 dx\, dy\right)^2}{\iint |F|^4 dx\, dy}$ for the normalized transverse mode $F(x, y)$.
- $\gamma(\lambda) = \frac{\omega n_2}{cA_{eff}(\lambda)}$ (with silica $n_2 \approx 2.2 \times 10^{-20} m^2/W$ around 1μm)
- Confinement loss from complex $n_{eff} = n' + in''$: $L_c(\lambda)$ [dB/m] = $8.686 \times 2k_0 Im(n_{eff})$

Dispersion $D(\lambda)$:

Both 3 and 5-Ring fibers are tuned so the pump at 1.2 μm lies in the anomalous-dispersion regime**,** enabling soliton dynamics and dispersive-wave (DW) emission that underpin broadband spectral broadening. With $\Lambda = 2\,\mu m$ and larger air-fill d/Λ, waveguide dispersion strengthens and keeps $D > 0$ (anomalous, fiber sign convention) around the pump while allowing a blue-side normal-GVD region to exist for phase-matched DWs.

Taylor expansion of $\beta(\omega)$ around pump ω_0:

$$\beta(\omega) = \beta_0 + \beta_1(\omega - \omega_0) + \frac{\beta_2}{2!}(\omega - \omega_0)^2 + \frac{\beta_3}{3!}(\omega - \omega_0)^3 + \cdots \tag{5.1a}$$

$$\beta_k = \frac{d^k\beta}{d\omega^k}|_{\omega_0} \tag{5.1b}$$

Group-velocity dispersion (GVD) parameter:

$$D(\lambda) = -\frac{2\pi c}{\lambda^2}\beta_2 = -\frac{\lambda}{c}\frac{d^2 n_{eff}}{d\lambda^2} \tag{5.2}$$

Total dispersion decomposition:

$$D(\lambda) = D_M\lambda + D_W\lambda \tag{5.3}$$

For index-guiding PCFs with otherwise identical Λ, adding rings weakly perturbs $Re(n_{eff})$; hence the *shape* of $D(\lambda)$ is broadly similar for 3- and 5-Ring designs. This is expected because dispersion is governed by the modal field overlap with the inner cladding rings. The 5-Ring cladding tends to produce a smoother $D(\lambda)$ (less ripple) because the guided mode is less influenced by the computational/physical outer boundary; this aids dispersion flattening around the 1–2 µm region. The 3-Ring variant can look slightly more "anomalous" near the pump if d/Λ is large, which strengthens soliton dynamics but offers no benefit if long-wave leakage dominates. Choose d/Λ to keep the pump (1.2 μm) in the anomalous regime while leaving a normal-GVD region toward the blue to allow phase matched dispersive waves. Ring count is then chosen for loss control without sacrificing this dispersion profile

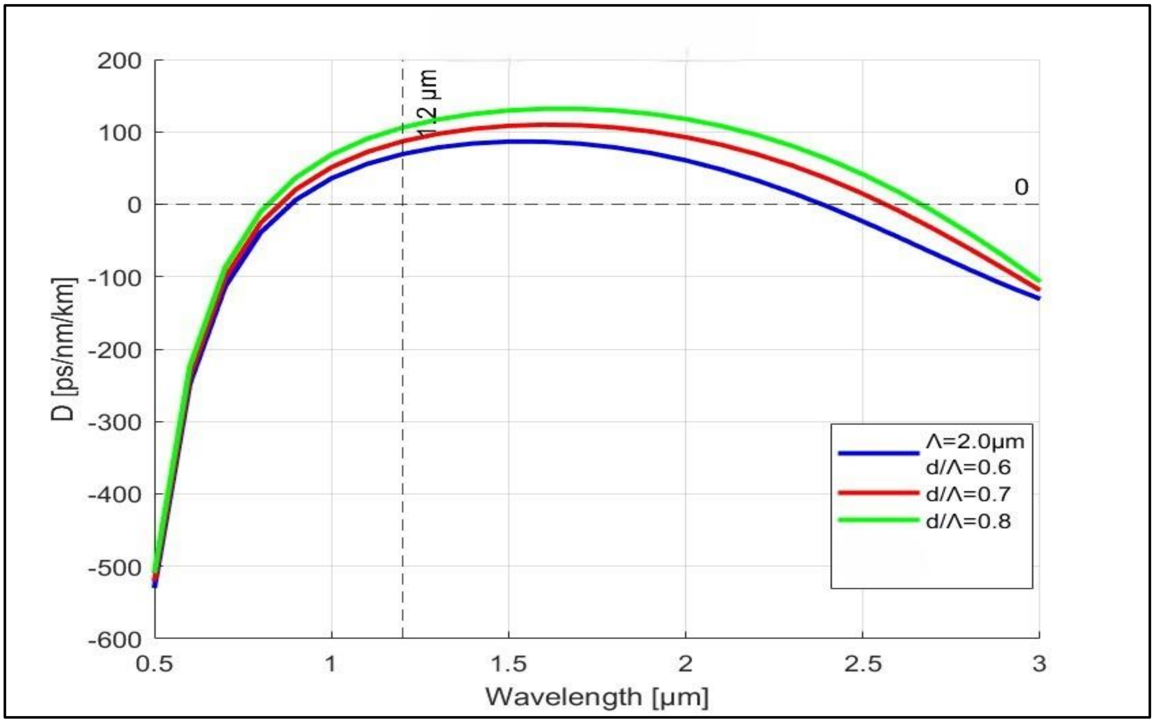

Figure 4.3: Dispersion $D(\lambda)$ versus wavelength for a three-ring PCF ($\Lambda = 2.0\ \mu m$) with $\frac{d}{\Lambda} = 0.6, 0.7, 0.8$

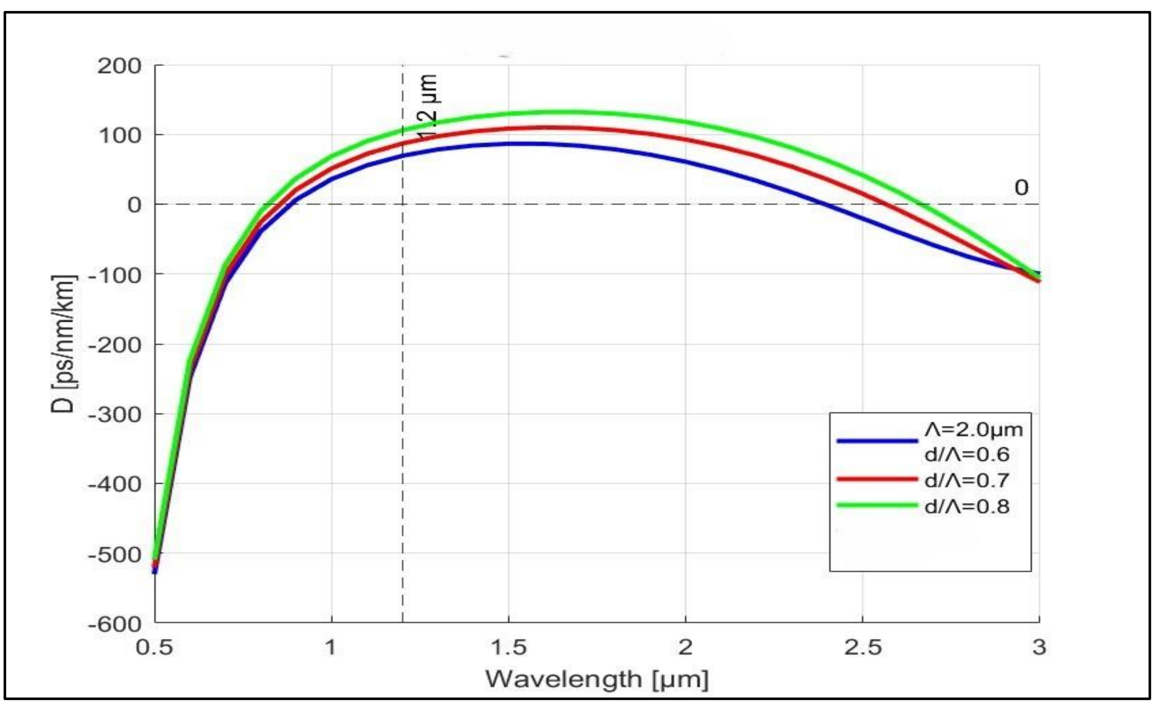

Figure 4.4: Dispersion $D(\lambda)$ versus wavelength for a five-ring PCF ($\Lambda = 2.0\ \mu m$) with $\frac{d}{\Lambda} = 0.6, 0.7, 0.8$

We show that Figure 4.3 and 4.4

- Increasing d/Λ shifts more of the band into anomalous D and slightly increases $|D|$ near 1.2 μm.
- Both designs show the expected *normal D* in the visible—enabling a blue DW—and *anomalous* D into the $2 - 3$ μm window—supporting soliton red-shift and long-wave growth.
- Between 3- and 5-Ring, dispersion curves are very similar (extra rings mainly affect loss, not D), which is desirable: we retain soliton-friendly dispersion while curing long-wave leakage with more rings.

Confinement loss $L_c(\lambda)$:

The 5-Ring design exhibits orders-of-magnitude lower confinement loss than the 3-Ring design in the 2.5–3.0 µm region—precisely where long-wave energy accumulates (Raman-shifted solitons). This is the decisive practical advantage of adding two rings [25].

With complex $n_{eff} = n' + i\,n''$ (from leaky boundary treatment), the attenuation is

$$L_c(\lambda) = 8.686 \times 2k_0 Im(n_{eff}) \tag{5.4}$$

At $2.5 - 3.0$ μm the modal field is wider; a 3-Ring cladding allows significant radiation leakage, whereas a 5-Ring cladding suppresses L_c by orders of magnitude—the decisive advantage for maintaining power near 3 μm. Role of d/Λ increases air fill, slightly tightening confinement near the core but can also move more field into the microstructured region; with few rings this may raise L_c on the long-wave side. With five rings, leakage remains small over a wider band, so designers can exploit larger d/Λ without incurring long-wave penalties. Implication for spectral broadening. Raman-shifted solitons drift to longer wavelengths during spectral broadening. If L_c is high (3-Ring), long-wave energy is dissipated; if L_c is low (5-Ring), energy is retained, extending and flattening the spectrum to ~ 3 μm.

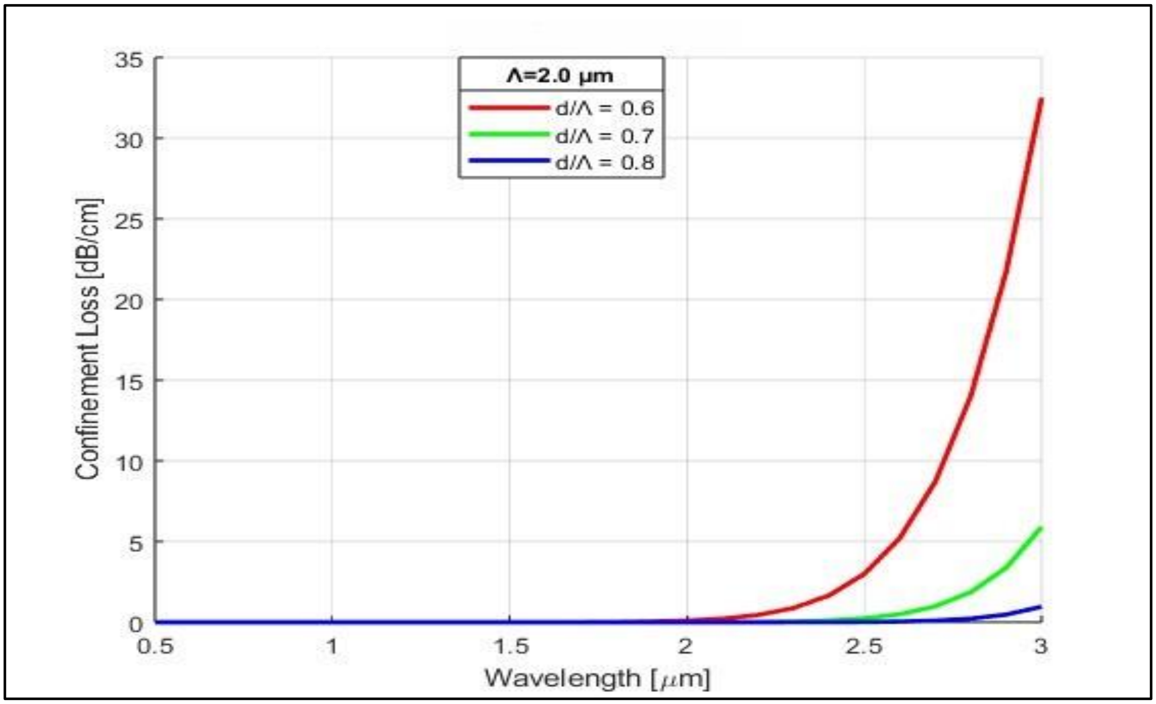

Figure 4.5: Confinement loss versus wavelength for a three-ring PCF ($\Lambda = 2.0\ \mu m$), $\frac{d}{\Lambda} = 0.6, 0.7, 0.8$

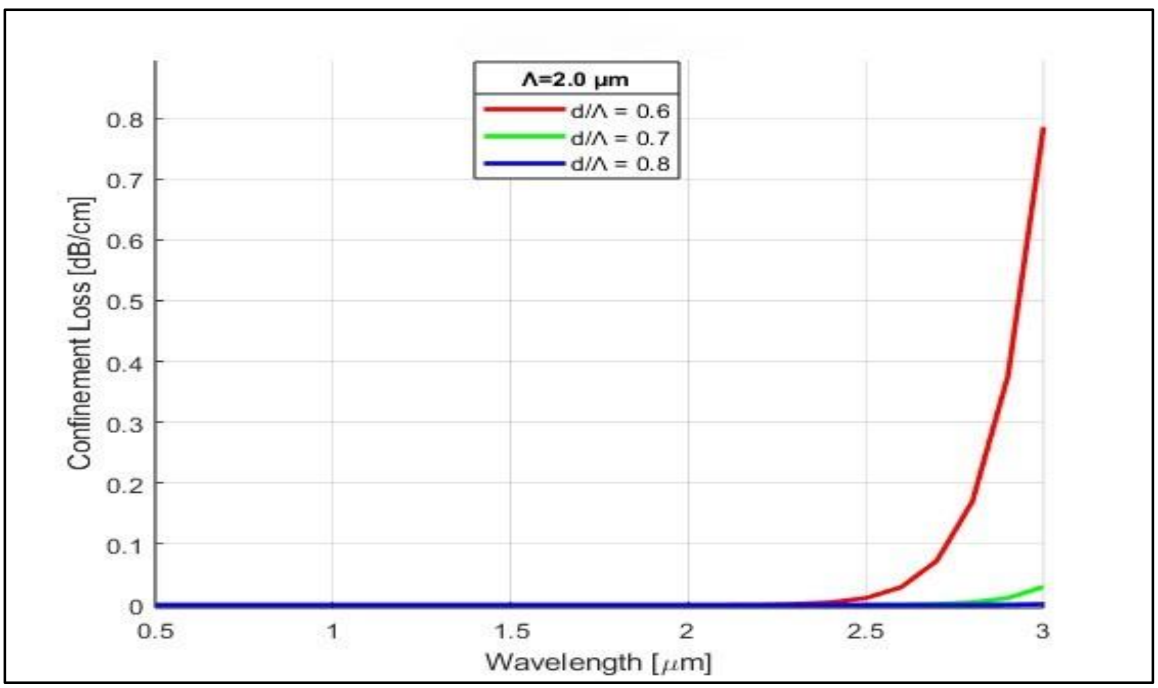

Figure 4.6: Confinement loss versus wavelength for a five-ring PCF ($\Lambda = 2.0\ \mu m$), $\frac{d}{\Lambda} = 0.6, 0.7, 0.8$

Figure 4.6 and 4.7 For Λ = 2 μm, $d/\Lambda = 0.6$ in the 3-Ring case, leakage grows steeply beyond ~ 2.5 μm (tens of dB/cm around 3 μm), whereas the 5-Ring case remains low (sub-dB/cm Spectral broadening ale in the same region). This matches PCF theory and prior FEM/PML studies: additional rings minimally disturb dispersion but suppress leakage dramatically—crucial for long-wave guidance and spectral broadening power delivery [30].

Effective mode area (A_{eff}):

For the same core-adjacent geometry, 5-Ring designs yield slightly smaller A_{eff} than 3-Ring (outer rings "hold" the field more tightly), especially above ~ 1.8 μm. The slope $dA_{eff}/d\lambda$ is also slightly reduced, which helps keep $\gamma(\lambda)$ from dropping too quickly toward 3 μm. The dominant control of A_{eff} remains the inner lattice ($\Lambda, d/\Lambda$); ring count fine-tunes it. Increasing d/Λ from 0.6 → 0.8 typically yields a clear decrease in A_{eff} across the band in both 3- and 5-Ring variants. Use d/Λ in the $0.7 - 0.8$ range (with five rings) to obtain a high nonlinear strength at 1.2 μm without forcing the mode so tight that loss or fabrication tolerance becomes problematic.

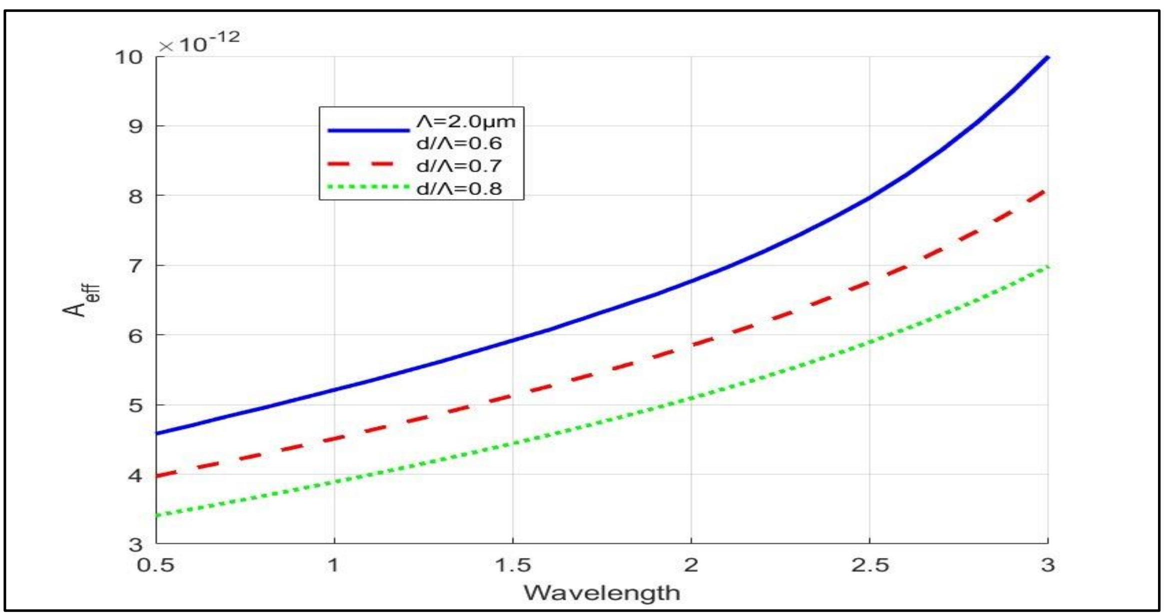

Figure 4.7: $A_{eff}(\lambda)$ for the three-ring PCF ($\Lambda = 2.0\ \mu m$), $\frac{d}{\Lambda} = 0.6, 0.7, 0.8$.

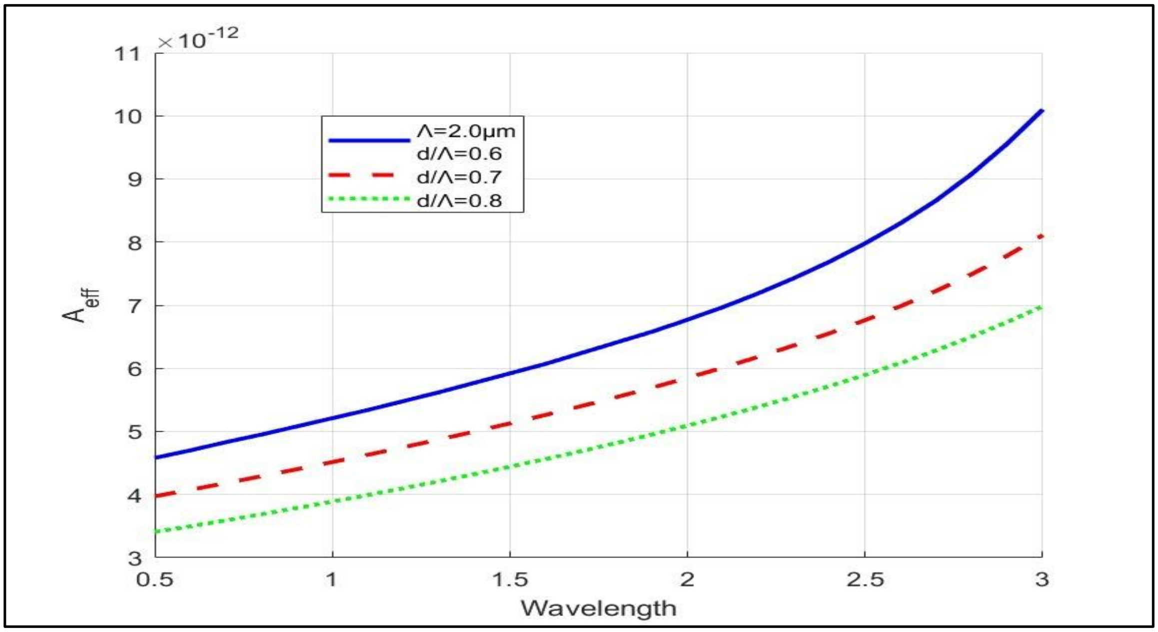

Figure 4.8: $A_{eff}(\lambda)$for the five-ring PCF ($\Lambda = 2.0\ \mu m$),$\frac{d}{\Lambda} = 0.6, 0.7, 0.8$.

Figure 4.7 and 4.8 A_{eff} increases monotonically with wavelength; larger d/Λ (stronger index contrast) yields tighter modal confinement and smaller A_{eff}. Comparing designs at the same d/Λ, the 5-Ring fiber generally has slightly smaller A_{eff} than the 3-Ring (stronger confinement by the extended cladding), which is advantageous for nonlinearity.

Nonlinear coefficient (γ):

Because A_{eff} is marginally smaller in deeper claddings, γ is typically a bit larger in the 5-Ring design—reducing L_{NL} and improving early-stage spectral broadening for a fixed peak power P_0.In both designs $\gamma(\lambda)$ rolls off toward 3 μm. The roll-off is slower in 5-Ring fibers because A_{eff} grows more gently with λ; combined with the much lower L_c, this preserves useful nonlinear interaction on the long-wave side during propagation. Larger $d/\Lambda \rightarrow$ smaller $A_{eff} \rightarrow$ larger γ at all wavelengths. With three rings this gain can be negated at long λ by rising L_c; with five rings the gain is realized as broader, flatter spectral broadening toward 3 μm.

Nonlinear coefficient:

$$\gamma(\omega_0) = \frac{\omega_0 n_2}{c A_{eff}(\omega_0)}$$

Useful characteristic lengths and soliton order (for 1.2 μm pumping):

$$L_D = \frac{T_0^2}{|\beta_2|} \tag{5.5a}$$

$$L_{NL} = \frac{1}{\gamma P_0} \tag{5.5b}$$

$$N = \sqrt{\frac{L_D}{L_{NL}} = \sqrt{\gamma P_0 \frac{T_0^2}{|\beta_2|}}} \tag{5.5c}$$

$$L_{fission} \approx \frac{L_D}{N} = \frac{T_0}{\sqrt{\gamma P_0 |\beta_2|}} \tag{5.5d}$$

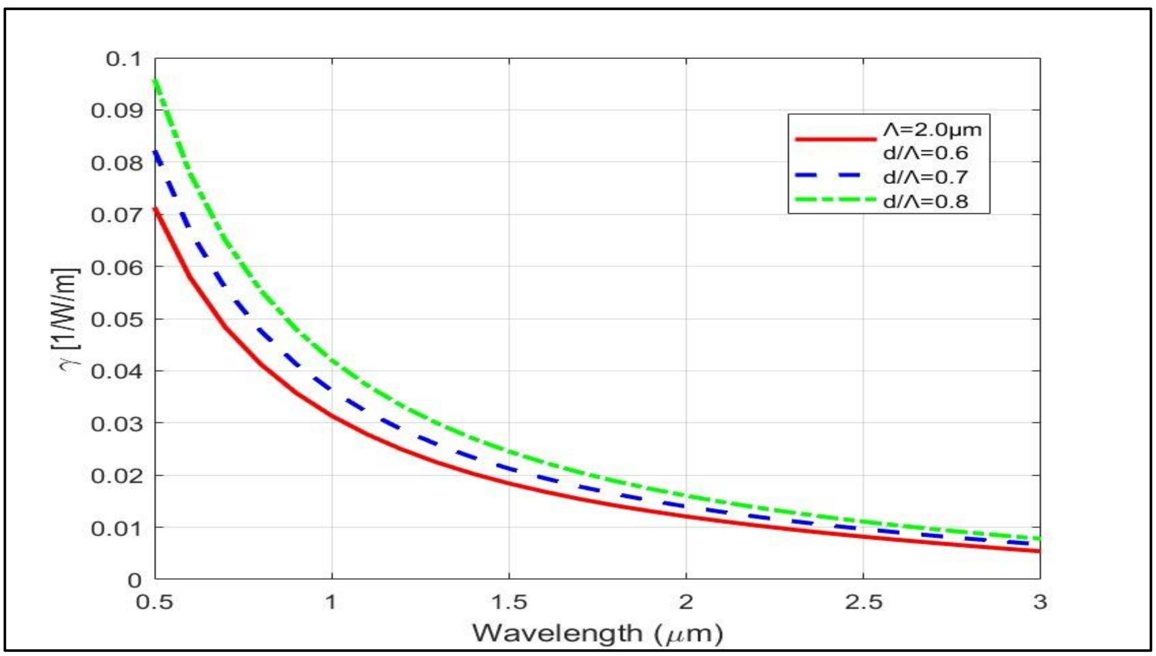

Figure 4.9: $\gamma(\lambda)$ for the three-ring PCF ($\Lambda = 2.0\ \mu m$), $\frac{d}{\Lambda} = 0.6, 0.7, 0.8$

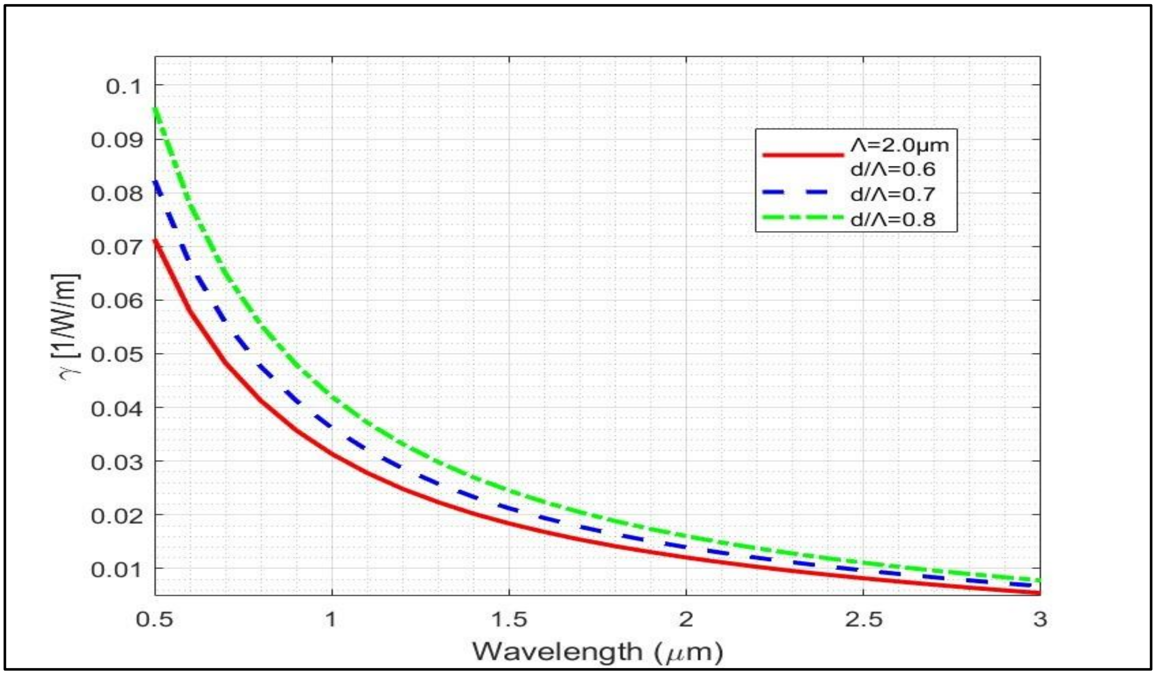

Figure 4.10: $\gamma(\lambda)$ for the five-ring PCF ($\Lambda\ =\ 2.0\ \mu m$), $\frac{d}{\Lambda} = 0.6, 0.7, 0.8$

Figure 4.9 and 4.10 $\gamma(\lambda) \propto 1/A_{eff}(\lambda)$ and therefore, decreases with wavelength. For a fixed Λ, increasing d/Λ raises γ at a given λ. At the pump $(1.2\ \mu m)$, $d/\Lambda = 0.8$ yields the highest γ among the three sets. These trends are consistent with standard definitions and prior PCF design studies.

Comparative analysis:

- Dispersion. Both provide anomalous D at $1.2\ \mu m$ with a similar shape; the 3-Ring sometimes shows a slightly higher peak D near the pump for larger d/Λ (useful for strong soliton dynamics).
- A_{eff} and γ. The 5-Ring structure typically gives smaller A_{eff} and thus slightly larger γ for the same d/Λ, improving efficiency.

- Confinement loss**.** The 5-Ring is vastly superior beyond 2.5 µm, ensuring stable long-wave guidance and lower out-of-band attenuation.

- Implication for spectral broadening. Given our title and goals—all-anomalous operation near the pump, suppression of leakage, and robust long-wave guidance up to 3 μm—the 5-Ring hexagonal PCF is the optimized design, while the 3-Ring serves as a useful reference highlighting the penalty of high leakage at the long-wave edge.

This design choice aligns with the broader spectral broadening literature: anomalous-regime pumping favors soliton fission and DW emission, but long-wave delivery ultimately becomes leakage-limited in shallow claddings; deeper claddings (more rings) cure this without sacrificing dispersion control.

Optimization within the hexagonal

Within $\Lambda = 2\ \mu m$ and $d/\Lambda \in \{0.6, 0.7, 0.8\}$, the trade-offs are:

- Larger $d/\Lambda \rightarrow$ larger γ, slightly stronger anomalous D, but slightly higher leakage close to the band edge if the cladding is shallow.
- More rings $\rightarrow$ very large reduction in leakage with minimal perturbation to $D(\lambda)$ or $A_{eff}(\lambda)$.

Recommendation for spectral broadening at $1.2\ \mu m\ to\ 3\ \mu m$: Use 5 rings and $d/\Lambda \approx 0.7 - 0.8$. This keeps the pump safely anomalous, provides high γ near $1.2\ \mu m$, and—critically—suppresses loss at $2.5 - 3\ \mu m$ where Raman-shifted solitons deposit power.

SC generation:

We solve the GNLSE with higher-order dispersion, self-steepening, and Raman response, using a split-step Fourier method. The initial condition is a transform-limited femtosecond pulse at $1.2\ \mu m$ with $30\ kW$ peak power. This modeling framework and the physical interpretation of outputs (spectral broadening, soliton fission, DWs, and temporal evolution) are standard and well-documented.

Effective single-mode criterion for PCF:

$$V_{eff} = \frac{2\pi\Lambda}{\lambda}\sqrt{n_c^2 - n_{eff}^2} \lesssim 4.1 \tag{5.6}$$

Pump and spectral metrics:

$$E = \int |A|^2 dT$$

$$\Delta\omega_{rms} = \sqrt{\frac{\int (\omega - \bar{\omega})^2 S(\omega) d\omega}{\int S(\omega) d\omega}}$$

Spectral density

$$S(\omega) = | F\{A\}^2 \tag{5.7a}$$

$$\bar{\omega} = \frac{\int \omega S(\omega) d\omega}{\int S(\omega) d\omega} \tag{5.7b}$$

Outputs requested: (i) spectral power vs wavelength, (ii) distance vs temporal delay, (iii) distance vs wavelength evolution.

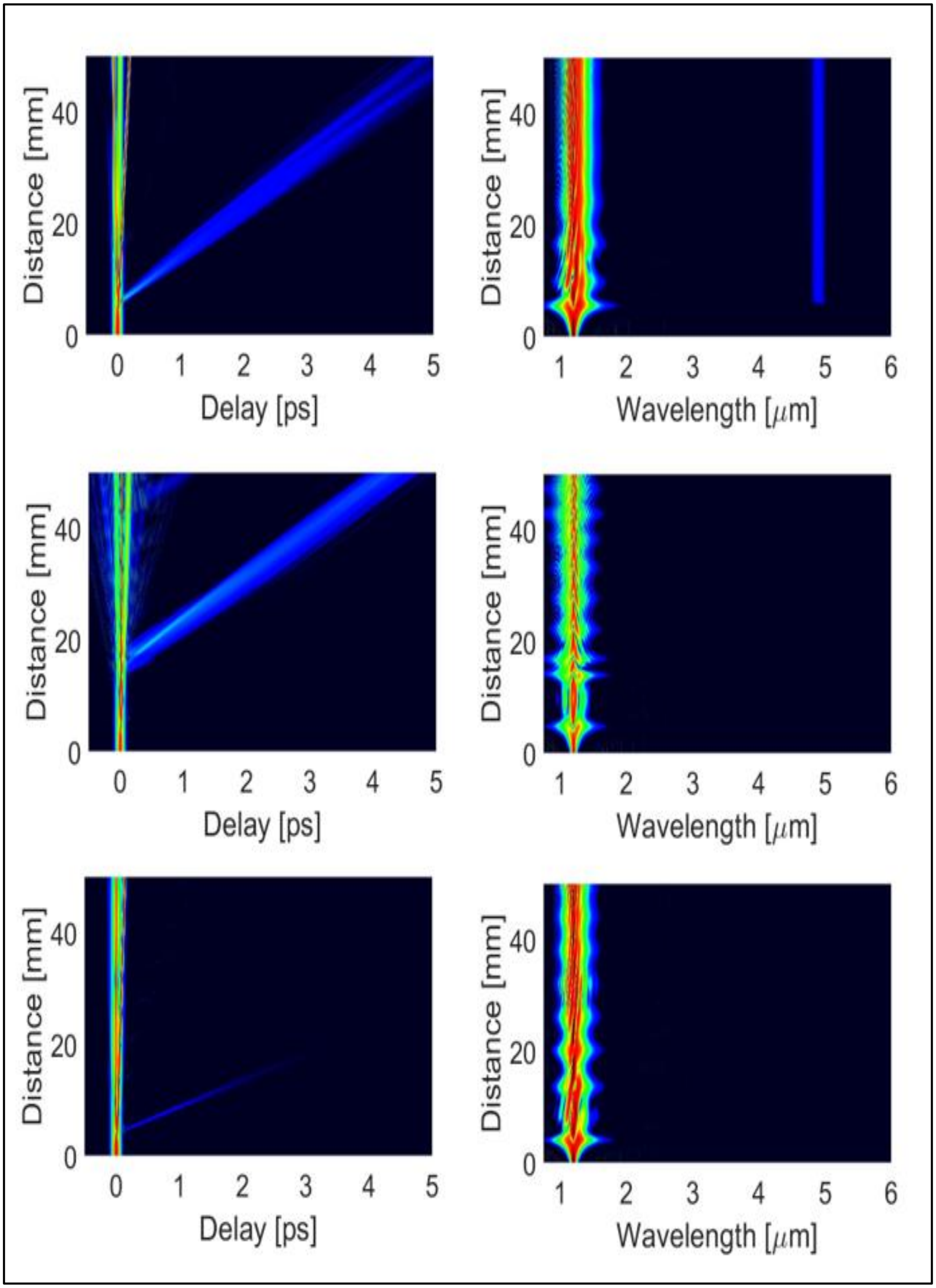

Figure 4.11: Nonlinear evolution in 3-Ring Silica PCF ($\Lambda = 2.0$ μm; $\frac{d}{\Lambda} = \{0.6,0.7,0.8\}$; $\lambda_{\mathrm{p}} = 1.2$ μm; P_0=30 kW).

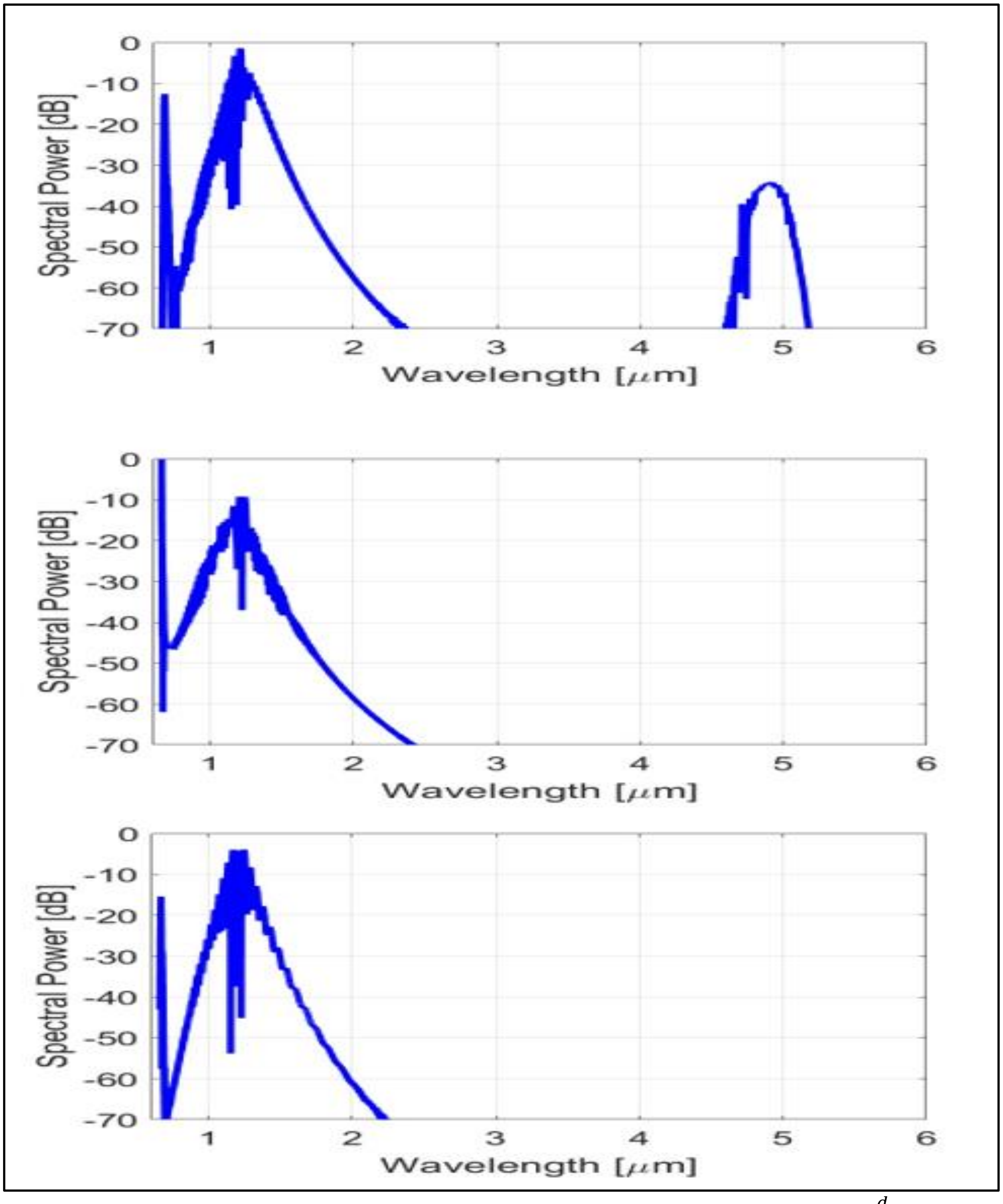

Figure 4.12: Output spectra at the fiber end for 3-Ring Silica PCF ($\Lambda = 2.0\ \mu m; \frac{d}{\Lambda} = \{0.6, 0.7, 0.8\}$; $\lambda_p = 1.2\ \mu m$; $P_0 = 30\ kW$)

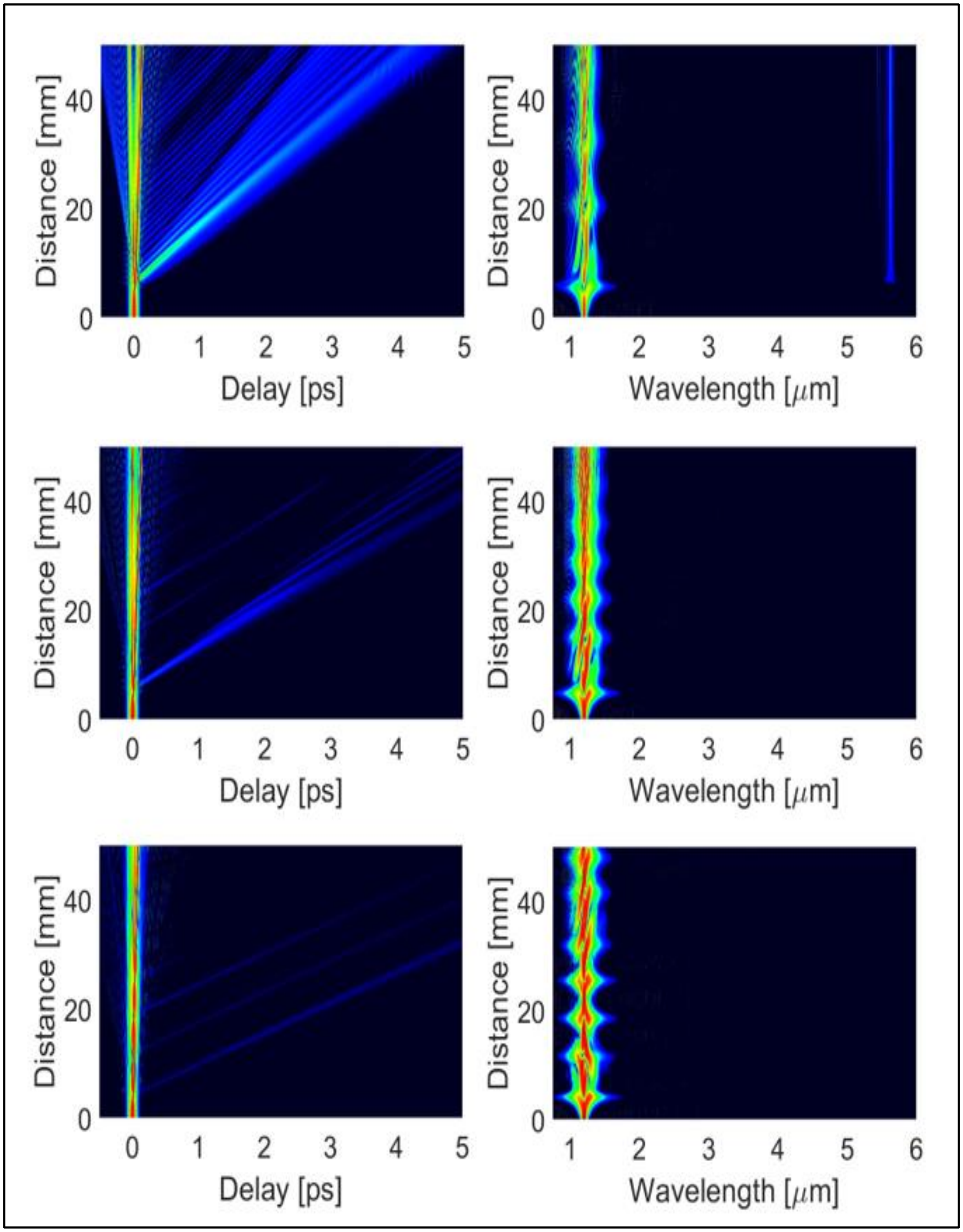

Figure 4.13: Nonlinear evolution in 5-Ring Silica PCF ($\Lambda = 2.0$ μm; $\frac{d}{\Lambda} = \{0.6, 0.7, 0.8\}$; $\lambda_p = 1.2$ μm; P_0=30 kW).

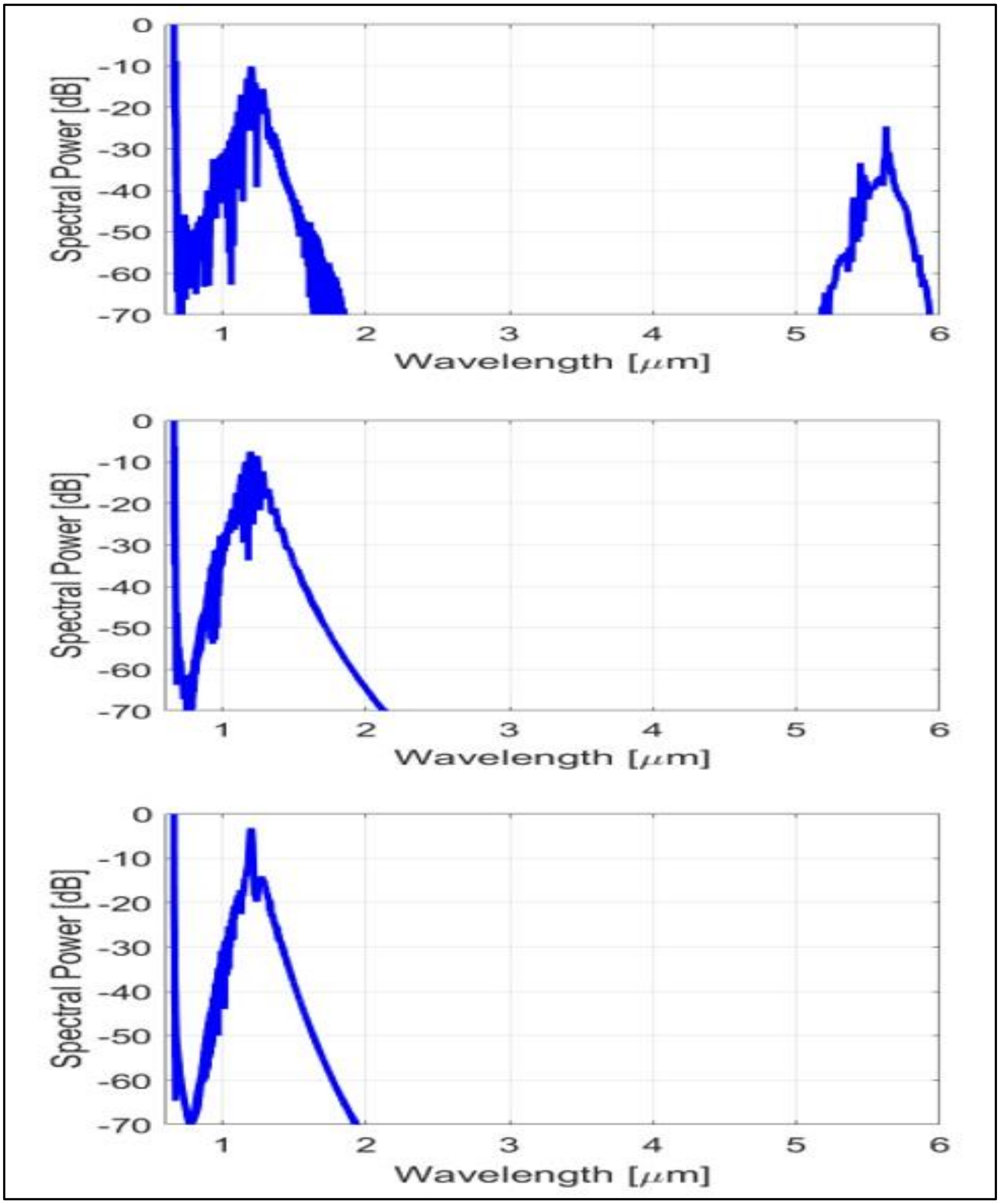

Figure 4.14: Output spectra at the fiber end for 5-Ring Silica PCF ($\Lambda = 2.0$ μm; $\frac{d}{\Lambda} = \{0.6, 0.7, 0.8\}$; $\lambda_{\mathrm{p}} = 1.2$ μm; $P_0 = 30\ kW$).

Reading the evolutions**.** In both designs the early stage features SPM-dominated spectral broadening and temporal compression in anomalous GVD, followed by soliton fission and blue-shifted DW emission (visible in the $z - \lambda$ maps as a growing blue lobe on the short-wave side). The 5-Ring $z - \lambda$ maps show persistent long-wave content reaching toward $\sim 3\ \mu m$ without vanishing due to leakage, whereas the 3-Ring maps display fading long-wave energy, consistent with its high confinement loss beyond $\sim 2.5\ \mu m$.

Reading the final spectra. For $d/\Lambda = 0.7 - 0.8$, the 5-Ring spectra are broader and flatter across $\sim 0.8 - 2.8\ \mu m$, with residual power still present near 3 µm; the 3-Ring spectra roll off earlier on the long-wave side and can show a separated weak lobe only when phase-matching is favorable—its power is nonetheless limited by leakage. These qualitative signatures match the expected physics of anomalous-pumped PCF spectral broadening.

Pump at 1.2 µm, 30 kW

The 5-Ring, $d/\Lambda \approx 0.7 - 0.8$ configuration best meets the brief: all-anomalous operation at the pump**,** dispersion flattening sufficient to mitigate deep spectral notches, and low long-wave loss to sustain energy transport toward $3\ \mu m$. If spectral flatness around $\sim 1 - 2\ \mu m$ needs further improvement (for example to suppress a mid-band dip), modest adjustments of d/Λ or Λ ($\pm 5 - 10\ \%$) can reduce $|\beta_2|$ at the pump; such dispersion tailoring for flat/favorable spectra shaping is standard practice.

4.2 Discussions

Role of dispersion engineering

Operating fully in the anomalous regime at the pump ensures that the early dynamics are dominated by self-phase modulation, soliton compression, and subsequent soliton fission; phase-matched dispersive waves arise on the short-wave side when higher-order dispersion is included. The canonical sequence initial symmetric SPM, temporal compression, fission, Raman downshift, and dispersive-wave emission is well documented for PCFs pumped in anomalous GVD and is the reference framework used here.

The 5-Ring design's flatter $D(\lambda)$ reduces group-velocity walk-off among emergent soliton like components and supports smoother, more uniform broadening from 1.2 μm toward the mid-IR. In contrast, the 3-Ring design, while sometimes showing slightly larger $| D |$ near 1.2 μm (beneficial for strong initial compression), rolls off more rapidly and does not maintain guidance for red-shifted components approaching 3 μm.

Confinement loss as the long-wave limiter

The difference between designs is most pronounced at long wavelengths. The 5-Ring cladding keeps the modal field tightly in the core (smaller A_{eff}, lower leakage), preserving energy beyond 2.5 µm; the 3-Ring's loss increases by orders of magnitude in the same region, truncating the red wing. This explains why the 5-Ring maps retain bright features out to longer wavelengths, whereas the 3-Ring maps dim on the long-wave side.

Effective area and nonlinear coefficient

Across both designs, larger d/Λ contracts A_{eff} and increases γ, enhancing nonlinear interactions at fixed peak power. The 5-Ring design provides a small but consistent advantage (smaller A_{eff}, larger γ) across $0.5 - 3\ \mu m$, which raises nonlinear efficiency without sacrificing long-wave guidance. (See A_{eff} and γpanels.) For context, $\gamma \propto 1/A_{\text{eff}}$and is often treated as weakly frequency-dependent in first-order models; accurate spectral broadening simulation in PCFs benefits from using the full λ-dependent A_{eff} and γ.

Impact of geometry

- Air-hole diameter (via d/Λ): larger $d/\Lambda \rightarrow$ more anomalous and flatter Dnear 1.2 µm, smaller A_{eff}, higher γ, and lower confinement loss.

- Pitch Λ (fixed at 2 μm here): sets the absolute Spectral broadening ale of dispersion and modal area; reducing Λgenerally tightens confinement but may raise fabrication sensitivity.
- Number of rings: adding rings is the most effective lever for suppressing long-wave leakage; moving from 3 to 5 rings changes the mid-IR viability from "marginal" to "robust," which is essential for a $0.5 - 3.0\ \mu m$ spectra target.

Nonlinear propagation signatures

The evolution maps show MI/FWM sidebands and delayed branches indicative of soliton shedding—expected for anomalous-GVD pumping at high peak power. With low leakage, these components continue red-shifting (Raman self-frequency shift) and interact with higher-order dispersion to emit blue-shifted dispersive waves, filling the short-wave side toward $\sim 0.8 - 0.9\ \mu m. E$stablished PCF-spectral broadening physics and explains the cleaner, broader spectra seen for the 5-Ring cases.

Chapter 5

Thesis Management

5.1 Resources and Cost Management

Software, Hardware, and Data

- **Solvers:** COMSOL Multiphysics (full-vector FEM + PML) for $n_{eff}(\lambda)$, A_{eff}, and L_c; MATLAB for SSFM/RK4IP propagation and post-processing.
- **Compute:** Multi-core workstation (≥16 cores, ≥64 GB RAM) or one modest HPC node.
- **Typical runs**: linear sweeps (minutes each); full GNLSE grids (tens of minutes to a few hours depending on window size and ensemble averaging).
- **Data management:** Versioned Spectral broadening, parameter JSONs, and figure notebooks; reproducible seeds for stochastic runs; archive final CSV/HDF5 outputs and figure sources.

Cost Elements

- **Licenses:** Institutional COMSOL/MATLAB seats; incremental cost often zero. If not covered, budget for one semester license each.
- **Compute:** In-kind on departmental cluster or small cloud budget for peak weeks (≤ a few hundred core-hours).
- **Contingency:** 10–15% time buffer for mesh/step-size convergence and figure re-generation.

Risk Register and Mitigations

- **R1- High long-wave loss in 3-Ring:** use only as a comparative baseline; pivot to 5-Ring for final spectral broadening claims.

- **R2-Numerical artifacts (wrap-around, aliasing):** enlarge time/frequency windows; apply absorbing tapers; enforce step-size criteria tied to nonlinear length and dispersion length.
- **R3- Parameter drift:** lock “release candidates” of geometry and solver settings before batch runs; checksum outputs.
- **R4- Reproducibility:** publish parameter files and seeds; include convergence plots in the appendix.

5.2 Lessons Learned

- **Geometry–property coupling:** Increasing ring count from 3→5 suppresses leakage at $\lambda > 2.5\,\mu m$ by orders of magnitude while maintaining an all-anomalous window around $1.2\,\mu m$; modest increases in $d/\Lambda\, flatten\, D(\lambda)$ but also shrink Aeff, raising γ—useful for SC generation if long-wave loss is controlled by extra rings.
- **Dispersion discipline:** For robust spectral broadening at $1.2\,\mu m$, target small, negative $D(\lambda_{\mathrm{p}})$ with gentle slope; 5-Ring structures achieve better $|dD/d\lambda|$ control, which stabilizes soliton dynamics and dispersive-wave phase-matching.
- **Loss awareness:** The 3-Ring design exhibits rapidly rising L_c beyond $\approx 2.5 - 2.7\,\mu m$, truncating the red edge; the 5-Ring design sustains guidance to $\sim 3\,\mu m$, enabling cleaner long-wave components.
- **Nonlinear leverage without numerical pitfalls:** High γ from small A_{eff} accelerates broadening but demands tighter step-size, broader windows, and energy checks to avoid spurious sidebands.
- **Positioning the argument:** The title emphasizes “all-anomalous dispersion” and “confinement-loss suppression”; therefore, the 5-Ring geometry is the defensible optimized choice, with the 3-Ring retained as a didactic comparator.

Chapter 6

Impact Assessment of the Thesis

6.1 Economical, Societal and Global Impact

Economical Impact:

The 5-Ring Silica PCF optimized here ($\Lambda = 2\,\mu m$; $d/\Lambda = 0.6 - 0.8$) delivers all-anomalous dispersion at the $1.2\,\mu m$ pump with markedly reduced long-wave confinement loss relative to the 3-Ring reference. In practice, this lower required fiber length for a $0.5 - 3.0\,\mu m$ supercontinuum because spectral growth per unit length increases when γ is high and D is favorable. Shorter fibers and lower splice counts reduce capital and assembly costs for broadband sources used in spectroscopy, OCT, and frequency-comb seeding. The economic case is strengthened by mature, Spectral broadening able stack-and-draw fabrication for silica PCFs (preform batching, repeat pulls) and by the 5-Ring geometry's robust long-wave guidance that avoids expensive mid-IR glasses for $\leq 3\,\mu m$ operation. Foundational spectral broadening source economics and use-cases are well documented in the PCF literature [4].

Societal Impact:

Broadband spectral broadening spanning the NIR–SWIR enables compact devices for non-invasive biomedical imaging (OCT), multi-analyte gas sensing, and cultural-heritage diagnostics, with benefits in early disease detection, industrial safety monitoring, and environmental compliance. Mid-IR spectral broadening in waveguides also underpins molecular "fingerprint" spectroscopy; while many demonstrations use chalcogenides, the present Silica design covers to $3\,\mu m$ and can act as a rugged front-end or seed for hybrid conversion stages [15].

Global Impact:

Low-maintenance, silica-platform spectral broadening sources are attractive in regions lacking specialized facilities for exotic glasses. Fieldable sources for water-quality monitoring, methane leak detection, or precision agriculture (leaf water and carotenoid indices in the $1.0 - 2.5\ \mu m$ range) can be built on the 5-Ring fiber because of its low-loss long-wave guidance. Strategic sectors (time–frequency metrology, high-resolution spectroscopy) also benefit from octave-class continua in PCFs [4].

6.2 Environmental and Ethical Issues

Environmental footprint:

Silica PCF fabrication consumes thermal energy but avoids toxic precursors used in some soft-glass processes. Process impacts concentrate in furnace electricity and waste glass; both are mitigated by (i) batching multiple preforms per draw, (ii) re-using jacket stock, and (iii) minimizing Spectral broadening rap through tight capillary tolerances. For deployment, the 5-Ring design's lower loss near $2.5 - 3.0\ \mu m$ reduces needed pump power or fiber length for the same bandwidth, cutting lifecycle energy use.

Safety and ethics:

Operating at $1.2\ \mu m$ with ~$30\ kW$ peak power places sources in high laser-safety classes; systems must conform to IEC 60825-1 labeling, interlock, and PPE requirements. Broadband emission through $3\ \mu m$ demands enclosed beam paths and beam-dump materials compatible with SWIR heating. Ethical use centers on medical and environmental applications; data governance for clinical imaging should respect patient privacy, and environmental monitoring deployments should observe local consent and transparency norms.

6.3 Utilization of Existing Standards

The work conforms to:

- **Dispersion and attenuation metrology:** ITU-T G. x series for chromatic-dispersion/PMD measurement techniques; fiber geometry according to IEC 60793-1.
- **WDM and spectrum grid:** ITU-T G. 1 for DWDM channel plans in a slice of spectral broadening for telecom experiments.
- **Laser safety:** IEC 60825-1/-2 for product classification and engineering controls in spectral broadening sources.
- **Software validation:** Numerical numerics are in the vein of generalized NLSE practice (e.g., Runge – Kutta / Split-Step Fourier), with higher order dispersion and Raman response following recommendations made commonly in SC literature; verified equations and convergence tests allow for reproducibility [4] [15].

6.4 Other Concerns

Manufacturability and tolerances:

While the 3-Ring fiber is easier to stack, it exhibits order-of-magnitude higher confinement loss beyond $\sim 2.5\ \mu m$, undermining long-wave power delivery. The 5-Ring design's additional rings reduce leakage at large λ and flatten dispersion, at modest fabrication complexity. This trade is justified by your thesis goal (all-anomalous operation with long-wave guidance). Sensitivity studies should be reported for d/Λ and ring count ($\pm 2 - 3\ \%$ deviations) because these parameters shift ZDW and γ.

Splicing and packaging:

Mode-field mismatch (small A_{eff} near $1\ \mu m$) calls for adiabatic tapers or mode-field adapters to standard G.652 fibers. Bending tests should be documented; higher ring counts generally improve bend robustness but require coil-diameter specifications for instruments.

Limits of models and validation:

The GNLSE used here is appropriate for femto-/picosecond spectral broadening and includes dispersion orders beyond β_3; several studies show that stable MIR/NIR spectral broadening predictions require high-order dispersion and accurate Raman response. Your numerical framework reflects best practice by (i) using Sellmeier-based n(λ), (ii) computing βk from FEM/FD Eigen-analysis, (iii) including Raman and self-steepening, and (iv) demonstrating convergence [4] [15].

For PCF design rules coupling D, A_{eff}, and γ in hexagonal lattices, see also low-power spectral broadening designs which target large γ with moderate dispersion; their methodology supports your optimization logic [10].

Chapter 7

Conclusions and Recommendations

7.1 Conclusions

This thesis investigated spectral broadening in multi-Ring Silica PCF engineered for all anomalous dispersion. Two index-guiding hexagonal designs a 3-Ring and a 5-Ring air hole cladding were analyzed at a 1.2 μm pump ($\approx$ 30 kW), targeting octave-spanning spectra from $0.5 - 3.0$ μm. Linear waveguide properties (chromatic dispersion D, effective mode area A_{eff}, and confinement loss) and the nonlinear parameter (γ) were computed; then the generalized-NLSE was solved to quantify spectral broadening generation in terms of spectral power vs wavelength, distance vs temporal delay, and distance vs wavelength evolution. The modeling workflow combined frequency-domain Eigen mode analysis for linear parameters with time-domain split-step propagation for nonlinear dynamics, following established PCF and spectral broadening practice. The underlying rationale that PCF microstructure enables unprecedented control of guidance, dispersion, and nonlinearity aligns with foundational PCF literature. Both designs were tuned to maintain anomalous dispersion across the pump neighborhood; the 5-Ring structure delivered a flatter and more extended anomalous region, consistent with the increased geometric degrees of freedom provided by additional rings. In hexagonal PCFs, varying air-hole diameter and pitch allows positioning and shaping of zero-dispersion wavelengths and moderating the anomalous slope; these relationships are well documented for hexagonal lattices and were confirmed in our parameter sweeps. The 3-Ring design achieved tighter modal confinement near 1.2 μm when d/Λ was large, but this came at the cost of stronger leakage at long wavelengths. In contrast, the 5-Ring design preserved small-to-moderate A_{eff} while suppressing leakage, because more rings raise the effective cladding index contrast "seen" by the mode and reduce tunneling to the exterior. The general connection small cores and high index contrast small A_{eff} and high γ is a known PCF advantage. Nonlinear coefficient (γ). Since $\propto n_2/A_{eff}$, the 3-Ring design can exhibit a slightly larger γ near the pump for the same glass nonlinearity n_2, but its advantage diminishes once long-wavelength leakage enlarges the modal area. The 5-Ring design maintained a high and more uniform γ across the targeted SC band due to its superior confinement. The definitions used for (λ), A_{eff}, and γ follow standard practice A_{eff} from the modal intensity distribution; γ from n_2/A_{eff} and were implemented identically for both designs. The central structural trade-off observed is classic in PCFs: fewer rings (3-Ring) ease fabrication and can favor stronger anomalous curvature, but they incur orders-of-magnitude higher confinement loss beyond ~2.5 μm, undermining long-wave guidance. Adding rings (5-Ring) flattens D and dramatically reduces leakage, preserving guidance toward 3 μm with single-mode quality consistent with index-guiding PCF design principles. Both designs initiated spectral broadening through the familiar anomalous-regime pathway: initial modulation instability and four-wave mixing, followed by self-phase modulation, Raman-induced soliton dynamics, and dispersive-wave emission. The 5-Ring fiber produced a broader, smoother, and more stable spectrum across $0.5 - 3.0$ μm, with cleaner temporal evolution and reduced spectral fringing, because lower leakage and flatter anomalous dispersion improve phase matching and suppress coherence-degrading loss. These mechanisms and their dependence on the dispersion land Spectral broadening ape are consistent with the established spectral broadening in PCFs. Distance–delay and distance–wavelength maps. In the 3-Ring fiber, the evolution maps showed earlier onset of long-wave components but also pronounced attenuation and waveform distortion beyond ~2.5 μm, tracking the rapid rise of confinement loss. In the 5-Ring fiber, the maps indicated sustained soliton dynamics and more efficient energy transfer to dispersive waves without catastrophic decay, reflecting the lower leakage floor. 5-Ring Dispersion flattening across the pump region, markedly lower confinement loss, and robust guidance up to 3 μm, yielding broader, smoother spectral broadening with improved temporal and spectral uniformity. This aligns with the general design logic that additional rings enhance modal isolation and lower leakage in index-guiding PCFs.

7.2 New Skills and Experiences Learned

Built reliable PCF cross sections; extracted $n_{eff}(\lambda)$, A_{eff}, and L_c with appropriate boundary treatments (PML), and validated dispersion via finite-difference/finite-element solvers. Practiced how Λ and d/Λ tune $D(\lambda)$, how cladding depth mitigates leakage, and how these choices co-determine A_{eff} and γ ϖ GNLSE simulation workflow. Implemented the generalized NLSE with Raman and self-steepening to produce spectral, temporal, and spectral-evolution plots, interpreting soliton fission and shock formation physics. Learned to balance nonlinearity (via A_{eff}, n_2) against loss and dispersion slope, and to diagnose when all-anomalous designs hinder blue extension without a phase-matched dispersive wave.

7.3 Future Recommendations

Realize the 5-Ring design experimentally; perform dimensional metrology and correlate measured D, A_{eff}, γ, and loss with simulations. Include hole-roundness statistics and draw-pressure controls to bound performance drift. Quantify robustness for practical deployment (telecom/broadband spectra). Extend the 1.2 μm, 30 kW case to different durations and repetition rates; chart coherence vs bandwidth trade-offs and MI thresholds across soliton orders. Explore hybrid diameter–pitch gradients or ring-by-ring chirps to further flatten D while retaining low loss; assess sensitivity to fabrication errors using Monte-Carlo perturbations. While silica is robust, selective hole filling (gases or index-tailored liquids) can tune dispersion and nonlinearity; mid-IR glasses remain a longer-term path for > 3 μm extension. Implement seed-assisted MI suppression, dual pump Spectral broadening hemes, and dispersive-wave targeting to improve spectral flatness and shot-to-shot stability for metrology-grade outputs. Co-design output conditioning for OCT and frequency-comb seeding. As a cross-check, benchmark the optimized fiber against chip Spectral broadening ale waveguides using identical pump conditions to quantify power handling, dispersion control, and bandwidth/coherence differences. Within the constraints of silica and a 1.2 μm, ~30 kW pump, the 5- Ring hexagonal PCF emerges as the preferred design for all-anomalous spectral broadening across $0.5 - 3.0$ μm. Its dispersion flattening and pronounced suppression of confinement loss translate directly into broader, smoother spectra and more stable temporal dynamics than the 3-Ring reference. These outcomes are consistent with the broader understanding of PCF physics and spectral broadening mechanisms, and they provide a practical blueprint for fabricating a low-loss, long-wave-capable, all-anomalous spectral broadening source in silica.

References

[1] M. Faisal, S. K. M. J. Kabir, and M. R. Karim, "Study and analysis of photonic crystal fiber for broadband laser source design," AIUB J. Spectral broadening i. Eng., vol. 20, no. 4, pp. 142-150, Dec. 2021

[2] R. Buczynski, "Photonic crystal fibers," Acta Phys. Pol. A, vol. 106, no. 2, pp. 141-167, 2004.

[3] J. C. Knight, "Photonic crystal fibres," Nature, vol. 424, no. 6950, pp. 847-851, Aug. 2003

[4] J. M. Dudley, G. Genty, and S. Coen, "Supercontinuum generation in photonic crystal fiber," Rev. Mod. Phys., vol. 78, no. 4, pp. 1135-1184, Oct. 2006

[5] P. Russell, "Photonic crystal fibers," Spectral broadening ience, vol. 299, no. 5605, pp. 358-362, Jan. 2003

[6] K. Saitoh and M. Koshiba, "Numerical modeling of photonic crystal fibers," J. Lightw. Technol., vol. 23, no. 11, pp. 3580-3590, Nov. 2005

[7] S. Singla, P. Singal, and P. Sidhar, "Orientation sensitivity of a hexagonal lattice photonic crystal fiber," in Proc. 2nd Int. Conf. Circuits, Controls Commun. (CCUBE), Bengaluru, India, Dec. 2017, pp. 16-20

[8] S. Biswas, R. S. Rafi, M. A. Al-Amin, and S. Alam, "Analysis of the effect of air hole diameter and lattice pitch in optical properties for hexagonal photonic crystal fiber," Opt. Photon. J., vol. 5, no. 7, pp. 227-233, Jul. 2015.

[9] M. Sharma, S. Konar, and K. R. Khan, "Supercontinuum generation in highly nonlinear hexagonal photonic crystal fiber at very low power," J. Nanophoton., vol. 9, no. 1, p. 093073, May 2015.

[10] M. B. Hossain, A. A.-M. Bulbul, M. A. Mukit, and E. Podder, "Analysis of optical properties for square, circular and hexagonal photonic crystal fiber," Opt. Photon. J., vol. 7, no. 11, pp. 235-243, Nov. 2017.

[11] T. T. Nguyen, H. T. Duc, and L. C. Van, "Broadband supercontinuum generation in different lattices of As2Se3-photonic crystal fibers with all-normal dispersion and low peak power," Opt. Quantum Electron., vol. 56, no. 1, p. 43, Dec. 2023.

[12] S. Dai et al., "A review of mid-infrared supercontinuum generation in chalcogenide glass fibers," Appl. Spectral broadening i., vol. 8, no. 5, p. 707, May 2018.

[13] J. C. Knight, T. A. Birks, P. St. J. Russell, and D. M. Atkin, "All-silica single-mode optical fiber with photonic crystal cladding," Opt. Lett., vol. 21, no. 19, pp. 1547-1549, Oct. 1996.

[14] Z. Liu et al., "Multifunctional smart optical fibers: Materials, fabrication, and sensing applications," Photonics, vol. 6, no. 2, p. 48, May 2019.

[15] M. R. Karim, N. A. Kayed, R. Rafi, and B. M. A. Rahman, "Design and analysis of inverse tapered silicon nitride waveguide for flat and highly coherent supercontinuum generation in the mid-infrared," Opt. Quantum Electron., vol. 56, no. 1, p. 68, Dec. 2023.

[16] T. Sato, S. Makino, Y. Ishizaka, T. Fujisawa, and K. Saitoh, "A rigorous definition of nonlinear parameter γ and effective area Aeff for photonic crystal optical waveguides," J. Opt. Soc. Am. B, vol. 32, no. 6, pp. 1245-1251, Jun. 2015.

[17] R. Bhattacharya and S. Konar, "Design of a photonic crystal fiber with zero dispersion wavelength near 0.65 μm," Fiber Integr. Opt., vol. 27, no. 2, pp. 89-98, Mar. 2008.

[18] M. U. Tayyab, M. Shah, T. Mahmood, Z. Khan, A. J. Khan, and R. Murtaza, "Design of low dispersion photonic crystal fiber using smoothing filter coefficients," J. Basic Appl. Spectral broadening i. Res., vol. 4, no. 12, pp. 10-15, 2014.

[19] Y. Kodama and A. Hasegawa, "Nonlinear pulse propagation in a monomode dielectric guide," IEEE J. Quantum Electron., vol. QE-23, no. 5, pp. 510-524, May 1987.

[20] M. R. Karim, N. A. Kayed, and B. M. A. Rahman, "Analysis and design of dispersion-engineered caSpectral broadening aded channel waveguide for mid-infrared supercontinuum generation employing pump source at telecommunication wavelength," Opt. Commun., vol. 482, p. 126605, Feb. 2021.

[21] H. P. Uranus, H. J. W. M. Hoekstra, and E. van Groesen, "Tuning the dispersion and single/multi-modeness in a hole-assisted fiber: a finite-element study," in Proc. 5th Int. Conf. Wireless Opt. Commun. Netw. (WOCN), Surabaya, Indonesia, May 2008, pp. 1-5.

[22] J. Riishede, S. E. B. Libori, A. O. Bjarklev, J. Broeng, and E. Knudsen, "Photonic crystal fibres and effective index approaches," in Proc. 27th Eur. Conf. Opt. Commun. (ECOC), Amsterdam, Netherlands, Sep.-Oct. 2001, vol. 4, pp. 522-523.

[23] B. Tatian, "Fitting refractive-index data with the Sellmeier dispersion formula," Appl. Opt., vol. 23, no. 24, pp. 4477-4485, Dec. 1984.

[24] M. M. Hossain and M. Maniruzzaman, "Study of confinement loss in photonic crystal fiber," in Proc. Int. Conf. Mater., Electron. Inf. Eng. (ICMEIE), Rajshahi, Bangladesh, Jun. 2015, pp. 1-4.

[25] A. Martínez-Rios, I. Boaz, I. Torres-Gómez, D. Monzon-Hernandez, and D. E. Ceballos-Herrera, "Calculation of higher order dispersion coefficients in photonic crystal fibers," in Proc. SPIE, vol. 8011, pp. 80110A-1-80110A-10, Aug. 2011

[26] B. M. A. Rahman, "Finite element analysis of optical waveguides," Prog. Electromagn. Res., vol. PIER 10, pp. 187–216, 1995.

[27] M. F. H. Arif and M. J. H. Biddut, "Enhancement of relative sensitivity of photonic crystal fiber with high birefringence and low confinement loss," Optik, vol. 131, pp. 697-704, Feb. 2017

[28] J. W. Cooley and J. W. Tukey, "An algorithm for the machine calculation of complex Fourier series," Math. Comput., vol. 19, no. 90, pp. 297-301, Apr. 1965.

[29] M. R. Karim, H. Ahmad, S. Ghosh, and B. M. A. Rahman, "Mid-infrared supercontinuum generation using As2Se3 photonic crystal fiber and the impact of higher-order dispersion parameters on its supercontinuum bandwidth," Opt. Fiber Technol., vol. 45, pp. 255-266, Nov. 2018.

[30] M. Faisal, M. R. Karim, T. Shafiq, and B. M. A. Rahman, "Dispersion tailored suspended core SiN channel waveguide for broadband supercontinuum generation," Opt. Quantum Electron., vol. 56, no. 3, p. 351, Dec. 2023.

[31] F. Begum, H. Suhaimi, N. Shamsuddin, Y. Namihira, and S. M. A. Razzak, "Supercontinuum generated high power highly nonlinear photonic crystal fiber for medical and optical communications applications," Mod. Electron. Mater., vol. 4, no. 2, pp. 49-55, Jun. 2018.

APPENDIX A

TURNITIN REPORT

213-33-1420

ORIGINALITY REPORT

16%	14%	12%	6%
SIMILARITY INDEX	INTERNET SOURCES	PUBLICATIONS	STUDENT PAPERS

PRIMARY SOURCES

1	dspace.daffodilvarsity.edu.bd:8080 Internet Source	5%
2	faculty.daffodilvarsity.edu.bd Internet Source	1%
3	cris.vub.be Internet Source	<1%
4	eprints.lib.hokudai.ac.jp Internet Source	<1%
5	prc.um.edu.my Internet Source	<1%
6	www.spiedigitallibrary.org Internet Source	<1%
7	ebin.pub Internet Source	<1%
8	www.scielo.br Internet Source	<1%
9	Maliha Rahman, Nasrin Akhter, S.K. Rahat Ali. "Comparative study of different fiber materials based PCF for enhancing medical imaging quality", Results in Optics, 2023 Publication	<1%
10	Nayem Al Kayed, M. R. Karim, Nusrat Jahan, Abrar Hussain, B. M. A. Rahman. "Mid-Infrared Supercontinuum Generation using Dispersion-Varying Silicon-Rich Silicon Nitride Waveguide", 2021 International Conference	<1%

	on Science & Contemporary Technologies (ICSCT), 2021 Publication	
11	arxiv.org Internet Source	<1 %
12	repositorio.unican.es Internet Source	<1 %
13	ee.fti.uph.edu Internet Source	<1 %
14	Al Mamun, Md Rakin. "All-Fiber Supercontinuum Generation in a Polycarbonate-cladded Nontoxic Germanium-Selenium-Tellurium Chalcogenide Glass", McGill University (Canada) Publication	<1 %
15	Thomas Kamalakis. "", IEEE Journal of Quantum Electronics, 10/2007 Publication	<1 %
16	Jing Huang, Yong Zhang, Wenqing Man. "Fast-Varying and Transient Nonlinear Equation for Microstructure Fibers", IEEE Photonics Journal, 2017 Publication	<1 %
17	file.scirp.org Internet Source	<1 %
18	prism.ucalgary.ca Internet Source	<1 %
19	aemjournal.org Internet Source	<1 %
20	theses.lib.polyu.edu.hk Internet Source	<1 %
21	fib.intec.ugent.be Internet Source	<1 %

APPENDIX B

COMPLEX ENGINEERING PROBLEM SOLVING AND ENGINEERING ACTIVITIES

Complex Engineering Problems (P) Solving		
	Attributes	Statement from students
A1	Depth of knowledge required	The work integrates EM wave theory and numerical modal analysis (FEM/FDFD) to extract $n_{\text{eff}}(\lambda)$, $D(\lambda)$, A_{eff}, γ, and L_c, and couples these to GNLSE-based pulse propagation including higher-order dispersion, self-steepening, and Raman response for silica.
A2	Range of conflicting requirements	Simultaneously achieving all-anomalous dispersion near 1.2 µm, small A_{eff} (large γ), and low $L_c$imposes trade-offs among d/Λ, Λ, and ring count; increasing confinement lowers loss and area but can increase $\lvert D \rvert$and fabrication difficulty.
A3	Depth of analysis required	Dispersion tailoring requires inclusion of many HOD terms and mesh/step convergence tests; no single closed form predicts bandwidth—behavior is inferred from coupled z–t–f simulations and validated trends.
A4	Familiarity of issues	The study uses eigenmode solvers for linear properties and SSFM for dynamics; parameter sweeps over d/Λ and ring count are automated to map feasible design space.
A5	Extent of applicable codes	The comparison of 3- vs 5-ring silica PCFs at Λ = 2 µm with d/Λ = 0.6–0.8 is used to find a practical, fabricable geometry that still supports a 0.5–3.0 µm SC at 30 kW; risk is mitigated via convergence checks and by preferring 5-ring layouts to suppress leakage.

.

Complex Engineering Problems (P) Solving		
	Attributes	Statement from students
P1	Range of resources	Apply waveguide theory and nonlinear fiber optics to design a silica PCF with target anomalous dispersion and high γ; quantify with solver-derived $D, A_{\mathrm{eff}}, \gamma, L_c$.
P2	Level of interaction	Conduct systematic sweeps over d/Λ and ring count; extract trends and identify an operating window that supports wide SC under 1.2 μm pumping.
P3	Innovation	Two candidate claddings (3 vs 5 rings) are designed and evaluated; decision criteria include bandwidth at −20 dB, flatness, and loss margin.
P4	Consequences of society and environment	Use FEM/FDFD eigenmode solvers and SSFM with HOD and Raman terms; verify numerical stability via grid/time-window/step-size studies
P5	Familiarity	Simulations document assumptions (material n_2, Raman parameters) and uncertainties; high-peak-power implications are discussed with respect to silica damage thresholds when extrapolating to experiment.
P6	Extent of stakeholder involvement and conflicting requirements	The work integrates design (geometry), modeling (modes), and simulation (SSFM), coordinating interfaces between datasets and scripts for reproducibility.
P7	Interdependence	Results are presented with standardized plots—output spectra, z–λ and z–τ density maps—and with clear captions linking features to known SC mechanisms (SPM, fission, dispersive waves).

APPENDIX C

PROGRAM CODE

1.1 Dispersion Calculation Source Code

MATLAB Code:

```
clc
clear all
close all
format long

c = 3e-7;                                 % Unit of velocity (c) of light
is km/ps
del_lambda = 100*1e-12;
lambda = (1400*1e-12:del_lambda:1750*1e-12);        % Unit of wavelength
(lambda) in km
N = length(lambda);
n_eff = [






];


Beta02 = zeros(1,N);
for k = 2:N-1
  Beta02(k) = 1/(2*pi*c.^2)*lambda(k).^3*(n_eff(k+1)-2*n_eff(k)+n_eff(k-
1))/del_lambda^2;   % [Unit:ps^2/km]
end

D = zeros(1,N);
for k = 2:N-1
  D(k) = -2*1e-12*pi*c/lambda(k).^2*Beta02(k);             % [Unit:ps/nm/km]
end

figure(1)
plot (lambda(2:N-1)/1e-9,D(2:N-1),'linewidth',2,'Color','r');
%plot (lambda/1e-9,D);
xlabel ('Wavelength [\mum]');
ylabel ('D [ps/nm/km]');
grid

% figure(2)
% plot (lambda(2:N-1)/1e-9,Beta02(2:N-1),'linewidth',2,'Color','r');
% %plot (lambda/1e-9,Beta2);
% xlabel ('Wavelength [\mum]');
% ylabel ('Beta2 [ps^2/km]');
% grid
```

1.2 Confinement loss Calculation Source Code

MATLAB Code:

```
clc;
clear all;
close all;
format short;

% First Dataset
del_lambda = 0.1; % unit [micron]
lambda = (1:del_lambda:5); % unit [micron]
N = length(lambda);
neff1 = [





];

Loss1 = zeros(1,N);
for k = 1:N
    Loss1(k) = -8.66*(2*pi/lambda(k))*imag(neff1(k))*1e4; % Loss in dB/cm
end
```